Available online at www.sciencedirect.com
SciVerse ScienceDirect
Geochimica et Cosmochimica 118 (2013) 98–117
Geochimica et Cosmochimica Acta
www.elsevier.com/locate/gca

Coupled sulfur and oxygen isotope insight into bacterial sulfate reduction in the natural environment

Gilad Antler [a,b,*], Alexandra V. Turchyn [b], Victoria Rennie [b], Barak Herut [c], Orit Sivan [a]

[a] Department of Geological and Environmental Sciences, Ben-Gurion University of the Negev, P. O. Box 653, Beer-Sheva 84105, Israel
[b] Department of Earth Sciences, University of Cambridge, Cambridge CB2 3EQ, UK
[c] Israel Oceanographic and Limnological Research, National Institute of Oceanography, Haifa 31080, Israel

Received 18 October 2012; accepted in revised form 3 May 2013; available online 14 May 2013

Abstract

We present new sulfur and oxygen isotope data in sulfate ($\delta^{34}S_{SO_4}$ and $\delta^{18}O_{SO_4}$, respectively), from globally distributed marine and estuary pore fluids. We use this data with a model of the biochemical steps involved in bacterial sulfate reduction (BSR) to explore how the slope on a $\delta^{18}O_{SO_4}$ vs. $\delta^{34}S_{SO_4}$ plot relates to the net sulfate reduction rate (nSRR) across a diverse range of natural environments. Our data demonstrate a correlation between the nSRR and the slope of the relative evolution of oxygen and sulfur isotopes ($\delta^{18}O_{SO_4}$ vs. $\delta^{34}S_{SO_4}$) in the residual sulfate pool, such that higher nSRR results in a lower slope (sulfur isotopes increase faster relative to oxygen isotopes). We combine these results with previously published literature data to show that this correlation scales over many orders of magnitude of nSRR. Our model of the mechanism of BSR indicates that the critical parameter for the relative evolution of oxygen and sulfur isotopes in sulfate during BSR in natural environments is the rate of intracellular sulfite oxidation. In environments where sulfate reduction is fast, such as estuaries and marginal marine environments, this sulfite reoxidation is minimal, and the $\delta^{18}O_{SO_4}$ increases more slowly relative to the $\delta^{34}S_{SO_4}$. In contrast, in environments where sulfate reduction is very slow, such as deep sea sediments, our model suggests sulfite reoxidation is far more extensive, with as much as 99% of the sulfate being thus recycled; in these environments the $\delta^{18}O_{SO_4}$ increases much more rapidly relative to the $\delta^{34}S_{SO_4}$. We speculate that the recycling of sulfite plays a physiological role during BSR, helping maintain microbial activity where the availability of the electron donor (e.g. available organic matter) is low.

1. INTRODUCTION

1.1. General

During the anaerobic oxidation of organic matter, bacteria respire a variety of electron acceptors, reflecting both the relative availability of these electron acceptors in the natural environment, as well as the decrease in the free energy yield associated with their reduction (Froelich et al., 1979). The largest energy yield is associated with aerobic respiration (O_2), then denitrification (NO_3^-), then manganese and iron reduction, followed by sulfate reduction (SO_4^{2-}) and finally fermentation of organic matter into methane through methanogenesis (Froelich et al., 1979; Berner, 1980). Due to the high concentration of sulfate in the ocean (at least two orders of magnitude more abundant than oxygen at the sea surface), dissimilatory bacterial sulfate reduction (BSR) is responsible for the majority of oxidation of organic matter in marine sediments (Kasten and Jørgensen, 2000). In addition, the majority of the methane produced during methanogenesis in marine sediments is oxidized anaerobically by sulfate reduction (e.g. Niewöhner et al., 1998; Reeburgh, 2007). The microbial utilization of

* Corresponding author at: Department of Earth Sciences, University of Cambridge, Cambridge CB2 3EQ, UK. Tel.: +44 (0)1223333479; fax: +44 (0)1223333450.
E-mail address: ga307@cam.ac.uk (G. Antler).

0016-7037
http://dx.doi.org/10.1016/j.gca.2013.05.005

sulfur in marine sediments is thus critical to the oxidation of carbon in the subsurface.

At a cellular level, the biochemical steps during BSR have been well studied over the past 50 years (Harrison and Thode, 1958; Kaplan and Rittenberg, 1964; Rees, 1973; Farquhar et al., 2003; Brunner and Bernasconi, 2005; Wortmann et al., 2007; Eckert et al., 2011; Holler et al., 2011). During BSR, bacteria respire sulfate and produce sulfide as an end product. This process consists of at least four major intracellular steps (e.g. Rees, 1973; Canfield, 2001a and Fig. 1): during step 1, the extracellular sulfate enters the cell; in step 2, the sulfate is activated with adenosine triphosphate (ATP) to form Adenosine 5′ Phosphosulfate (APS); in step 3, the APS is reduced to sulfite (SO_3^{2-}); and in step 4 the sulfite is reduced to sulfide. It is generally assumed that all four steps are reversible (e.g. Brunner and Bernasconi, 2005; Eckert et al., 2011). The reduction of sulfite to sulfide (step 4) remains the most enigmatic, and may occur in one step with the enzyme dissimilatory sulfite reductase or through the multi-step trithionite pathway producing several other intermediates (e.g. trithionate ($S_3O_6^{2-}$) and thiosulfate ($S_2O_3^{2-}$) – Kobayashi et al., 1969; Brunner et al., 2005; Sim et al., 2011a; Bradley et al., 2011); although there is evidence that whatever pathway step 4 occurs through, it is also reversible (Trudinger and Chambers, 1973; Trudinger and Chambers, 1973;Eckert et al., 2011; Holler et al., 2011; Tapgaar et al., 2011).

Given that each of the four steps is reversible, understanding the relative forward and backward fluxes at each step and how these fluxes relate to the overall rate of sulfate reduction, is critical for understanding the link between the BSR and the rate of organic matter oxidation. Changes in environmental conditions (e.g. temperature, carbon substrate, pressure) likely impact the relative forward and backward fluxes at each step within the cell as well as the overall rate of BSR, but the relative role of these factors with respect to one another in the natural environment remains elusive. Within the marine subsurface, measurements of sulfate concentrations in sedimentary pore fluids and subsequent diffusion-consumption modeling of the rate of sulfate depletion with depth can be used for calculating the overall rate of sulfate reduction below the ocean floor (e.g. Aller and Blair, 1996; Berner, 1980; D'Hondt et al., 2004; Wortmann, 2006; Wortmann et al., 2007). These sulfate concentration profiles alone, however, cannot provide details about how the individual biochemical steps at a cellular or community level may vary with depth or under different environmental conditions.

A particularly powerful tool for studying these biochemical steps during BSR (hereafter termed the 'mechanism' of BSR) is sulfur and oxygen isotope ratios measured in the residual sulfate pool while sulfate reduction progresses (Mizutani and Rafter, 1973; Fritz et al., 1989; Böttcher et al., 1998; Aharon and Fu, 2000, 2003; Brunner et al., 2005; Turchyn et al., 2006, 2010; Wortmann et al., 2007; Farquhar et al., 2008; Aller et al., 2010). With respect to isotopes, we refer to the ratio of the heavier isotope of sulfur or oxygen (^{34}S or ^{18}O) to the lighter isotope (^{32}S or ^{16}O), reported in delta notation relative to a standard (VCDT for sulfur and VSMOW for oxygen) in parts per thousand or permil (‰).

Although both sulfur and oxygen isotopes are partitioned during each intracellular step, their relative behavior (e.g. $\delta^{18}O_{SO_4}$ vs. $\delta^{34}S_{SO_4}$) in the natural environment is not fully understood. The sulfur isotope composition of sulfate ($\delta^{34}S_{SO_4}$) typically increases monotonically as BSR progresses (e.g. Harrison and Thode, 1958; Kaplan and Rittenberg, 1964; Rees, 1973). This occurs because most of the enzymatic steps during BSR preferentially select the lighter sulfur isotope (^{32}S), slowly distilling it into the produced sulfide pool and leaving ^{34}S behind. The magnitude of the sulfur isotope partitioning (fractionation) during the overall process of BSR can be as high as 72‰ (Wortmann et al., 2001; Brunner and Bernasconi, 2005; Sim et al., 2011a). Theoretical and experimental studies have suggested that this magnitude is a function of microbial metabolism and carbon source (e.g. Brüchert, 2004; Sim et al., 2011b), amount of sulfate available (e.g. Canfield, 2001b; Habicht et al., 2002), and temperature (e.g. Brüchert et al., 2001; Canfield et al., 2006). In addition, previous studies also noted a relationship between the magnitude of the sulfur isotope fractionation and the sulfate reduction rate (Kaplan and Rittenberg, 1964; Rees, 1973; Chambers et al., 1975). This relationship has been shown in pure culture experiments (e.g. Canfield et al., 2006), batch culture experiments using natural populations (e.g. Stam et al., 2011) and

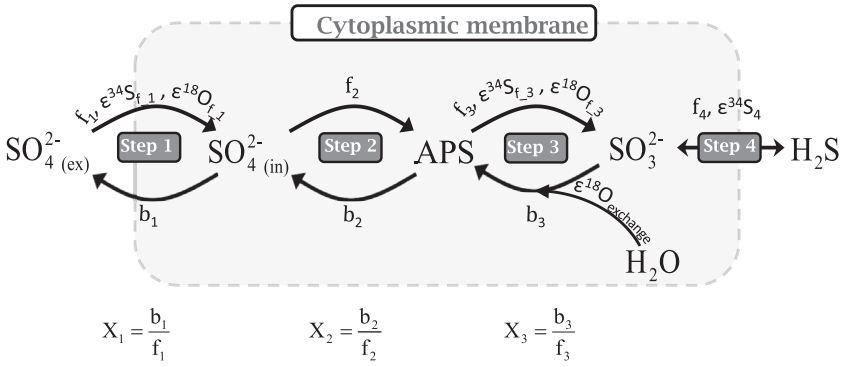

Fig. 1. The steps of bacterial sulfate reduction and the potential of oxygen and sulfur isotopic fractionations. $i_{\_j}$, $\varepsilon^{34}S_{i\_j}$ and $\varepsilon^{18}O_{i\_j}$ are the flux and the fractionation effect for sulfur and oxygen, respectively, for the forward ($i = f$) and backward ($i = b$) reaction j ($j = 1,\ldots,4$). X_k ($k = 1$, 2 and 3) is the ratio between the backward and forward fluxes.

calculated *in situ* using pore fluids profiles (e.g. Aharon and Fu, 2000; Wortmann et al., 2001); in all these studies, higher sulfur isotope fractionation corresponded to slower sulfate reduction rates.

On the other hand, the $\delta^{18}O_{SO_4}$ has shown variable behavior during BSR in natural environments. In some cases, the $\delta^{18}O_{SO_4}$ exhibits a linear relationship with $\delta^{34}S_{SO_4}$, also suggesting a distillation of the light isotope from the reactant sulfate. The magnitude of the oxygen isotope fractionation during this distillation was suggested to be 25% of the magnitude for sulfur isotopes (Mizutani and Rafter, 1969), although it has been observed to range between 22% (Mandernack et al., 2003) and 71% (Aharon and Fu, 2000). In most measurements of $\delta^{18}O_{SO_4}$ during BSR in the natural environment, however, the $\delta^{18}O_{SO_4}$ increases initially until it reaches a constant value and does not increase further, while the $\delta^{34}S_{SO_4}$ may continue to increase (e.g. Fritz et al., 1989; Böttcher et al., 1998, 1999; Turchyn et al., 2006; Wortmann et al., 2007; Aller et al., 2010; Zeebe, 2010). This 'oxygen isotope equilibrium' value (usually between 22‰ and 30‰ in most natural environments) has been shown to depend on the $\delta^{18}O$ of the ambient water (Mizutani and Rafter, 1973; Fritz et al., 1989; Brunner et al., 2005; Mangalo et al., 2007, 2008). Because the timescale for oxygen isotope exchange between sulfate and water is exceptionally slow (e.g. Lloyd, 1968; Chiba and Sakai, 1985; Zak et al., 1980.), it has been suggested that, during BSR, oxygen isotopes of sulfur intermediate species such as APS and SO_3^{2-} exchange oxygen atoms with water (Mizutani and Rafter, 1973; Fritz et al., 1989). Recent studies have suggested that it is more likely sulfite when bound in the AMP-sulfite complex facilitates this oxygen isotopic exchange (Kohl and Bao, 2006; Wortmann et al., 2007; Brunner et al., 2012; Kohl et al., 2012). This requires that some percentage of the sulfate that is brought into the cell does not get reduced all the way to sulfide but undergoes oxygen isotope exchange with water, reoxidation to sulfate, and release back to the extracellular sulfate pool (Mizutani and Rafter, 1973; Fritz et al., 1989; Brunner et al., 2005, 2012; Mangalo et al., 2007, 2008; Wortmann et al., 2007; Farquhar et al., 2008; Turchyn et al., 2010).

Interpreting the relative evolution of the $\delta^{18}O_{SO_4}$ and the $\delta^{34}S_{SO_4}$ in the extracellular sulfate pool during BSR in natural environments, and what this relative evolution tells us about the enzymatic steps during sulfate reduction remains confounding. Fig. 2 shows schematically how pore fluid sulfate and sulfur and oxygen isotope profiles often look in nature, where pore fluid sulfate concentrations decrease below the sediment–water interface and the oxygen and sulfur isotope ratios of sulfate increase, but may evolve differently relative to one another. One question is what are the factors controlling BSR in natural environments when the coupled sulfur and oxygen isotopes increase linearly (Trend A), compared to when they are decoupled and oxygen isotopes are seen to plateau (Trend B)? A second problem is that the majority of our understanding of the biochemical steps during BSR comes from pure culture studies; how does this understanding translate, if at all, to the study of BSR in the natural environment?

In this paper we will forward this discussion by presenting a compilation of sulfur and oxygen isotopes in pore fluids, including seven new sites collected over a range of different subsurface marine and near-marine environments, covering a broad range of sulfate reduction rates. This will allow us to investigate how the relative behavior of the sulfur and oxygen isotopes varies in these different environments. We will begin with a discussion of modeling sulfur and oxygen isotope evolution during BSR, most of which is a review of previous seminal work. We will then discuss how these models for the biochemical steps during BSR can be applied to pore fluids in the natural environment. Finally, we will present our results, along with a compilation of previously published data into the context of our model.

1.2. Kinetic and equilibrium isotope effects on sulfur and oxygen isotopes during dissimilatory bacterial sulfate reduction (BSR)

The overall sulfur and oxygen isotope fractionation during BSR should be the integration of the various forward and backward fluxes at each step with any corresponding isotope fractionation at each step, be it kinetic or equilibrium (Fig. 1 and Rees, 1973). In this section we will outline the previous modeling efforts and the related equations, upon which our model (Section 2) is based. We begin with sulfur isotopes, which have been more extensively studied than oxygen isotopes. The total sulfur isotope fractionation was first calculated by Rees (1973):

$$\varepsilon^{34}S_{total} = \varepsilon^{34}S_{f\_1} + X_1 \cdot (\varepsilon^{34}S_{f\_2} - \varepsilon^{34}S_{b\_1}) + \ldots$$
$$X_1 \cdot X_2 \cdot (\varepsilon^{34}S_{f\_3} - \varepsilon^{34}S_{b\_2}) + X_1 \cdot X_2 \cdot X_3 \cdot (\varepsilon^{34}S_{f\_4} - \varepsilon^{34}S_{b\_3}) \quad (1)$$

where $\varepsilon^{34}S_{total}$ is the total expressed sulfur isotope fractionation, $\varepsilon^{34}S_{i\_j}$ is the sulfur isotope fractionation during the forward ($i = f$) and backward ($i = b$) reaction j (where $j = 1,\ldots,4$) and X_k (where $k = 1, 2, 3$) is the ratio between the backward and forward fluxes of the respective intracellular steps (Fig. 1). The overall expressed sulfur isotope fractionation in the residual sulfate pool, according to this model, is always dependent on the isotope fractionation in the first step (the entrance of sulfate into the cell). The fractionation during the subsequent steps can be expressed in the residual sulfate pool only if there is a backward reaction at each step and a flux of sulfate back out of the cell. The overall expressed sulfur isotope fractionation has been linked to various environmental factors that must result in changes in the relative forward and backward fluxes at each step (Rees, 1973; Farquhar et al., 2003, 2007; Brunner and Bernasconi, 2005; Canfield et al., 2006; Johnston et al., 2007).

The sulfur isotope fractionation for the forward reaction at steps 1, 3 and 4 (Fig. 1), that is, sulfate incorporation into the cell, the reduction of APS to sulfite, and the reduction of sulfite to sulfide, are understood to be −3‰, 25‰ and 25‰ respectively (all others steps are assumed to have no sulfur isotope fractionation, Rees, 1973). Therefore, Eq. (1) can be written as:

$$\varepsilon^{34}S_{total} = -3‰ + X_1 \cdot X_2 \cdot 25‰ + X_1 \cdot X_2 \cdot X_3 \cdot 25‰ \quad (2)$$

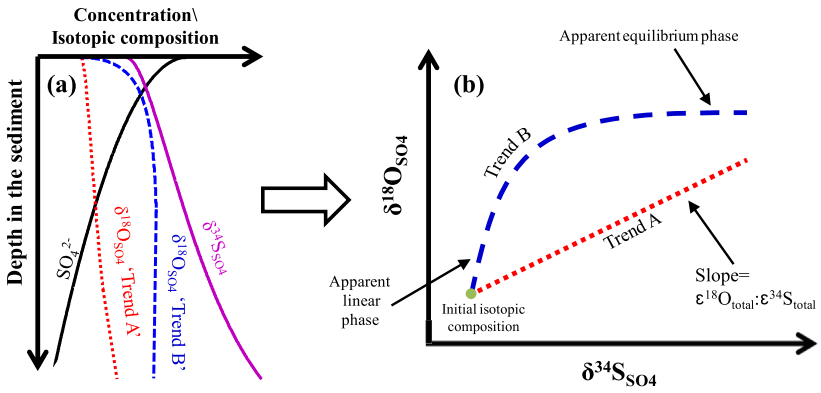

Fig. 2. Schematic possible behavior of sulfate during bacterial sulfate reduction as SO_4^{-2}, $\delta^{18}O_{SO_4}$ and $\delta^{34}S_{SO_4}$ profiles (a) and $\delta^{18}O_{SO_4}$ vs. $\delta^{34}S_{SO_4}$ (b). 'Trend A' shows that $\delta^{18}O_{SO_4}$ and $\delta^{34}S_{SO_4}$ increase at a constant ratio, while sulfate reduction propagates with depth (e.g. Aharon and Fu, 2000). 'Trend B' shows an increase in $\delta^{34}S_{SO_4}$ and $\delta^{18}O_{SO_4}$ values at the onset of the curve, $\delta^{18}O_{SO_4}$ reaches equilibrium values as sulfate reduction prorogates with depth while $\delta^{34}S_{SO_4}$ continue to increase.

In order to generate an expressed sulfur isotope fractionation larger than −3‰, there must be back reactions during at least the first three steps. It has also been observed that the total expressed sulfur isotope fractionation during BSR decreases with increased sulfate reduction rates (e.g. Aharon and Fu, 2000; Canfield et al., 2006; Stam et al., 2011; Sim et al., 2011b). This suggests, as previous research has concluded, that as the sulfate reduction rate increases, backward reactions become less significant relative to forward reactions, and the total sulfur isotope fractionation approaches the fractionation associated with transfer of sulfate through the cell wall (Canfield, 2001a,b).

Eq. (2) predicts a maximum possible expressed sulfur isotope fractionation during BSR of 47‰. However, particularly in natural environments, the measured sulfur isotope fractionation can often exceed these values, reaching up to 72‰ (Habicht and Canfield, 1996; Wortmann et al., 2001). Such large offsets are often attributed to repeated redox cycles of sulfur in the subsurface: the initial reduction of sulfate through BSR, the subsequent reoxidation of sulfide to elemental sulfur, followed by sulfur disproportionation to sulfate and sulfide, which produces more sulfate for BSR (Canfield and Thamdrup, 1994). These repeated cycles allow for a larger overall expressed sulfur isotope fractionation. Another explanation for the large sulfur isotope fractionations observed in nature is the trithionite pathway, in which the reduction of sulfite to sulfide (step 4) proceeds through multiple steps rather than one (Kobayashi et al., 1969; Brunner and Bernasconi, 2005; Johnston et al., 2007; Bradley et al., 2011; Sim et al., 2011a). This could induce additional sulfur isotope fractionation and result in expressed sulfur isotope fractionation as large as 72‰ (Brunner and Bernasconi, 2005; Sim et al., 2011a).

Defining a relationship like Eq. (1) for oxygen isotopes is somewhat more difficult because both kinetic oxygen isotope fractionation and equilibrium oxygen isotope fractionation need to be considered. If we first consider the case where kinetic oxygen isotope fractionation is the only process affecting $\delta^{18}O_{SO_4}$ during BSR, then the overall oxygen isotope fractionation can be formulated similar to Eq. (1) (Brunner et al., 2005):

$$\varepsilon^{18}O_{total} = \varepsilon^{18}O_{f\_1} + X_1 \cdot (\varepsilon^{18}O_{f\_2} - \varepsilon^{18}O_{b\_1}) + \ldots$$
$$X_1 \cdot X_2 \cdot (\varepsilon^{18}O_{f\_3} - \varepsilon^{18}O_{b\_2}) + X_1 \cdot X_2 \cdot X_3 \cdot (\varepsilon^{18}O_{f\_4} - \varepsilon^{18}O_{b\_3}) \quad (3)$$

In this case, the $\delta^{18}O_{SO_4}$ and $\delta^{34}S_{SO_4}$ in the residual sulfate pool will evolve in a similar manner and a linear relationship should emerge when plotting one isotope versus the other ('Trend A' in Fig. 2). The ratio between $\varepsilon^{18}O_{total}$ and $\varepsilon^{34}S_{total}$ would then be equal to the slope of this line.

However, the $\delta^{18}O_{SO_4}$ also exhibits equilibrium oxygen isotope fractionation during BSR, often linked to the isotopic composition of the ambient water (Mizutani and Rafter, 1973; Fritz et al., 1989; Brunner et al., 2005, 2012; Mangalo et al., 2007, 2008; Farquhar et al., 2008; Turchyn et al., 2010; Zeebe, 2010). Field studies have found that this 'equilibrium isotope exchange' results in the $\delta^{18}O_{SO_4}$ in the residual sulfate pool evolving to a value between 22‰ and 30‰, across a range of natural environments (Böttcher et al., 1998, 1999; Turchyn et al., 2006; Wortmann et al., 2007; Aller et al., 2010). The fact that the $\delta^{18}O_{SO_4}$ reaches a constant value is interpreted as oxygen isotope exchange between intracellular sulfur intermediates and water. The measured oxygen isotope equilibrium value therefore includes the kinetic oxygen isotope fractionation associated with each step, the equilibrium partitioning of oxygen isotopes between intracellular water and the intermediate sulfur species, and any oxygen isotope fractionation associated with the assimilation of oxygen atoms from water during reoxidation. Because of the myriad of factors impacting the observed equilibrium value of $\delta^{18}O_{SO_4}$, the measured value in the residual sulfate $\delta^{18}O_{SO_4}$ is termed the 'apparent equilibrium' (Wortmann et al., 2007). Turchyn et al. (2010) formulated a mathematical term for the apparent equilibrium of $\delta^{18}O_{SO_4}$, assuming full isotope equilibrium between intra-cellular intermediates and water, and kinetic oxygen isotope fractionation only during the reduction of APS to sulfite (step 3):

$$\delta^{18}O_{SO_4(A.E)} = \delta^{18}O_{H_2O} + \varepsilon^{18}O_{exchange} + \frac{1}{X_3} \cdot \varepsilon^{18}O_{f\_3} \quad (4)$$

where $\delta^{18}O_{SO_4(A.E)}$ is the isotopic composition of sulfate at 'apparent equilibrium', $\delta^{18}O_{H_2O}$ is the isotopic composition of the ambient water, $\varepsilon^{18}O_{exchange}$ is the oxygen isotope fractionation between sulfite in the AMP-sulfite complex and ambient water, X_3 is the ratio between the backward and forward fluxes at Step 3 as in Eq. (1) (Fig. 1) and $\varepsilon^{18}O_{f\_3}$ is the kinetic oxygen isotope fractionation associated with APS reduction to sulfite.

In summary, current models for BSR suggest that sulfur and oxygen isotopes in the residual sulfate pool respond to changes in the relative forward and backward rates of reaction, and isotope fractionation associated with each step during BSR. The relative contribution of these various forward and backward fluxes and their individual isotope fractionation should be expressed by different relationships between $\delta^{18}O_{SO_4}$ and $\delta^{34}S_{SO_4}$ in sulfate as BSR progresses. When the kinetic oxygen isotope fractionation outcompetes the equilibrium oxygen isotope fractionation, the plot of $\delta^{18}O_{SO_4}$ vs. $\delta^{34}S_{SO_4}$ should exhibit a linear relationship ('Trend A' in Fig. 2b – e.g. Mizutani and Rafter, 1969; Aharon and Fu, 2000, 2003; Mandernack et al., 2003). When the equilibrium isotope effect dominates, a plot of $\delta^{18}O_{SO_4}$ vs. $\delta^{34}S_{SO_4}$ will tend concavely towards the 'apparent equilibrium' ('Trend B' in Fig. 2b – e.g. Böttcher et al., 1998, 1999; Turchyn et al., 2006; Aller et al., 2010). In between these two extremes, the relative intensity of the kinetic and equilibrium isotopic effects will determine the moderation of the curve and how quickly it reaches equilibrium, if at all.

It has been suggested that this relative evolution of the $\delta^{18}O_{SO_4}$ vs. $\delta^{34}S_{SO_4}$ during BSR should be connected to the overall sulfate reduction rate (Böttcher et al., 1998, 1999; Aharon and Fu, 2000; Brunner et al., 2005) where the steeper the slope on a plot of $\delta^{18}O_{SO_4}$ vs. $\delta^{34}S_{SO_4}$, the slower the sulfate reduction rate. This suggestion was elaborated upon by Brunner et al. (2005), who formulated a model for mass flow during BSR. In this work, Brunner et al. (2005) deduced that the overall SRR is important for the relative evolution of $\delta^{18}O_{SO_4}$ and $\delta^{34}S_{SO_4}$, but that the rate of oxygen isotope exchange between sulfur intermediates and water, and the relative forward and backward fluxes at each step further modifies the evolution of $\delta^{18}O_{SO_4}$ vs. $\delta^{34}S_{SO_4}$.

The above models as developed previously have applied largely to understanding the relative forward and backwards steps during BSR in pure culture. We hypothesize that we can investigate a wider range of sulfate reduction rates in the natural environment, and thus are poised to be able to address this relationship more completely. This is a particularly good juncture to investigate this further as the models for BSR and the relationship between the mechanism and the couple sulfate isotopes have experienced several significant advances in recent years (e.g. Brunner et al., 2005, 2012; Wortmann et al., 2007). Although there are potentially other processes in natural environments that may impact the measured $\delta^{18}O_{SO_4}$ vs. $\delta^{34}S_{SO_4}$ – for example anaerobic pyrite oxidation (e.g. Balci et al., 2007; Brunner et al., 2008; Heidel and Tichomirowa, 2011; Kohl and Bao, 2011), or sulfur disproportionation (Cypionka et al., 1998; Böttcher et al., 2001, 2005; Böttcher and Thamdrup, 2001; Aharon and Fu, 2003; Blake et al., 2006; Aller et al., 2010), we feel there is significant knowledge to be gained by revisiting the mechanism of BSR as deduced from geochemical analysis of pore fluids.

The use of the evolution of the $\delta^{18}O_{SO_4}$ vs. $\delta^{34}S_{SO_4}$ to inform the biochemical steps during BSR has been applied in two previous studies. Wortmann et al. (2007) produced a detailed study of an ODP site off the coast of southern Australia and Turchyn et al. (2006) studied 11 ODP sites off the coasts of Peru, Western Africa and New Zealand. Both studies found a rapid increase in the $\delta^{34}S_{SO_4}$, while the $\delta^{18}O_{SO_4}$ increased and then leveled off (similar to 'Trend B' in Fig. 2). Both Wortmann et al. (2007) and Turchyn et al. (2006) used their data with reactive transport models to calculate the relative forward and backward fluxes through bacterial cells during BSR. These studies, which greatly advanced our understanding of *in situ* BSR, focused on deep-sea sediments, with necessarily slow sulfate reduction rates. Furthermore, both of these studies considered only one branching point within the microbial cell, whereas more recent models of the mechanism of BSR have invoked the importance of at least two branching points to help explain the decoupled sulfur and oxygen isotopes during BSR (Brunner et al., 2005, 2012).

In this paper, we will present sulfur and oxygen isotopes of pore fluid sulfate from seven new sites with sulfate reduction rates that span many orders of magnitude. We will combine our new data with previously published results of subsurface environments where sulfur and oxygen isotopes in sulfate have been reported. We will use a model derived from the equations above, to understand how the relative evolution of sulfur versus oxygen isotopes in pore fluid sulfate inform us about the intracellular pathways and rates involved in BSR.

2. MODEL FOR OXYGEN ISOTOPE DURING BSR

2.1. The proposed model for oxygen isotopes in sulfate

Our model for oxygen isotopes in sulfate is derived from the work of Brunner et al. (2005, 2012). In order to understand the relative evolution of sulfur and oxygen isotopes in sulfate during BSR in pure culture, Brunner et al. (2005, 2012) solved a time dependent equation in which the oxygen isotope exchange between sulfur intermediates and ambient water and the cell specific sulfate reduction rates are the ultimate factors controlling the slope of $\delta^{18}O_{SO_4}$ vs. $\delta^{34}S_{SO_4}$ during the onset of BSR. For the purpose of this study (as applied to natural environments rather than pure cultures) we reconsider this model in three ways. First, the cell specific sulfate reduction rate varies over orders of magnitudes in different natural environments, yet the relative evolution of $\delta^{18}O_{SO_4}$ vs. $\delta^{34}S_{SO_4}$ plot versus depth may exhibit the same pattern. Therefore, we suggest that any time dependent process related to the isotope evolution (e.g. the rate of the oxygen isotopic exchange between ambient water and sulfur intermediate such as sulfite) is faster than the other biochemical steps during BSR. Second, in the

models of Brunner et al. (2005, 2012) the equilibrium value for the $\delta^{18}O_{SO_4}$ depended critically on the value of $\delta^{18}O$ of the ambient water. However, the equilibrium value for $\delta^{18}O_{SO_4}$ in natural environments shows a range (22–30‰) that cannot be explained only by the variation in $\delta^{18}O$ of the ambient water (which ranges from 0‰ to −4‰). It was initially suggested that these equilibrium values may reflect oxygen isotope equilibrium at different temperatures (Fritz et al., 1989) although more recent studies have shown that the temperature effect is small (~2‰ between 23 and 4 °C – Brunner et al., 2006; Zeebe, 2010). Temperature may impact the relative intracellular fluxes during BSR (Canfield et al., 2006), and this will change the apparent equilibrium value (Turchyn et al., 2010). For our model, therefore, we attribute the change in the $\delta^{18}O_{SO_4}$ to change in the mechanism of the BSR and not to changes in the $\delta^{18}O$ of the water. Third, the model of Brunner et al. (2005, 2012) ruled out a linear relationship between $\delta^{18}O_{SO_4}$ and $\delta^{34}S_{SO_4}$ which has not been observed in pure culture. Our model will need to account for a linear relationship, which has been observed in natural environments.

To address these issues, we remove the characteristic timescale used by Brunner et al. (2005, 2012) for the cell-specific sulfate reduction rate and focus instead on how the different fluxes at each step impact the evolution of $\delta^{18}O_{SO_4}$ vs. $\delta^{34}S_{SO_4}$. We further allow changes in the equilibrium values of the $\delta^{18}O_{SO_4}$ due to a combination of equilibrium and kinetic oxygen isotope effects (apparent equilibrium) rather than through a change in the $\delta^{18}O$ of the ambient water.

The assumptions in our model include:

- The system is in steady state. This means SRR $= f_i - b_i$ (where $i = 1, 2, 3$—Fig. 1).
- We model oxygen isotopic exchange between ambient water and the sulfite (Betts and Voss, 1970; Horner and Connick, 2003), recognizing that this exchange may occur when sulfite is already bound in the AMP-sulfite complex. This oxygen isotope exchange contributes three oxygen atoms to the sulfate that will ultimately be produced during reoxidation, while the fourth oxygen atom is gained during the reoxidation of the AMP-sulfite complex to sulfate (Wortmann et al., 2007; Brunner et al., 2012).
- Oxygen isotopic exchange was considered to be much faster with respect to other biochemical steps, which means, that for any practical purpose, the sulfite is constantly in isotopic equilibrium with the ambient water. This results in a solution that is independent of the timescale of the problem. This is because the timescale for this isotope exchange, given intracellular pH (6.5–7—Booth, 1985), should shorter than minutes (Betts and Voss, 1970).
- The kinetic oxygen isotopic fractionation during the reduction of APS to sulfite (f_3) is equal to 25% of the sulfur isotope fractionation ($\varepsilon^{18}O_{f\_3}$: $\varepsilon^{34}S_{f\_3} = 1{:}4$) (Mizutani and Rafter, 1969). This value for the kinetic oxygen isotope fractionation is the lowest value that was found in lab experiments, and therefore we consider it to be the closest to the real ratio between $\varepsilon^{18}O_{f\_3}$ and $\varepsilon^{34}S_{f\_3}$. This is assumption has not been made by Brunner et al. (2005, 2012) and allows our model to simulate a linear relationship between $\delta^{18}O_{SO_4}$ and $\delta^{34}S_{SO_4}$.
- Any kinetic oxygen isotope fractionation in step 4 (the reduction of sulfite to sulfide) is not significant for oxygen isotopes, since oxygen isotope exchange during the back reaction (step 3) resets the $\delta^{18}O$ of the sulfite.
- We simplified step 4 by making it unidirectional. We are able to do this because recent work has suggested that even if sulfide concentrations are high (>20 mM), only ~10% of the sulfide is re-oxidized (Eckert et al., 2011) which is insignificant with respect to the overall recycling of other sulfur intermediates (Turchyn et al., 2006; Wortmann et al., 2007).

The full derivation of the model equations using these assumptions, and similar to the derivation in Brunner et al., 2012, is in Appendix A and yields the following continuous solution for $\delta^{18}O_{SO_4(t)}$ as function of $\delta^{34}S_{SO_4(t)}$:

$$\delta^{18}O_{SO_{4(t)}} = \begin{cases} \frac{\varepsilon^{18}O_{total}}{\varepsilon^{34}S_{total}} \cdot (\delta^{34}S_{SO_{4(t)}} - \delta^{34}S_{SO4(0)}); + \delta^{18}O_{SO_4(0)}; \\ X_1 \cdot X_2 \cdot X_3 = 0 \\ \delta^{18}O_{SO_{4(A.E)}} - \exp(-\theta_0 \cdot \frac{\delta^{34}S_{SO_{4(t)}} - \delta^{34}S_{SO_{4(0)}}}{\varepsilon^{34}S_{total}}) \cdot \\ (\delta^{18}O_{SO_{4(A.E)}} - \delta^{18}O_{SO_{4(0)}}); \quad 0 < X_1 \cdot X_2 \cdot X_3 < 1 \end{cases} \tag{5}$$

where $\delta^{18}O_{SO_4(t)}$ is the oxygen isotopic composition of the residual sulfate at time t, $\delta^{18}O_{SO_4(A.E)}$ is the oxygen isotopic composition of the residual sulfate at apparent equilibrium (see Section 1.2 above) and $\delta^{18}O_{SO_4(0)}$ is the oxygen isotope composition of the initial sulfate. The $\delta^{34}S_{SO_4(t)}$ is the sulfur isotopic composition of the residual sulfate at time t, $\delta^{34}S_{SO_4(0)}$ is the initial sulfur isotopic composition of the residual sulfate, $\varepsilon^{34}S_{total}$ $\varepsilon^{18}O_{total}$ are the overall expressed sulfur and oxygen isotope fractionation, respectively, and θ_0 is a parameter initially formulated by Brunner et al. (2005, 2012). This parameter (θ_0) measures the ratio between the apparent oxygen isotope exchange and sulfate reduction rate. However, since we assumed constantly full oxygen isotopic equilibrium between sulfite and ambient water, in our case this parameter should only be a function of the ratio between the backward and forward fluxes, and is less impacted by changes in the initial isotopic composition of the sulfate, the isotopic composition of the water, the kinetic isotope fractionation factor for step 3, or the magnitude of the fractionation factor during oxygen isotopic exchange (see Appendix A).

The solution to our model (Eq. (5)) suggests two distinct phases for the relative evolution of $\delta^{18}O_{SO_4}$ vs. $\delta^{34}S_{SO_4}$ during BSR:

(1) *Apparent linear phase*. This phase refers to the initial stage of BSR, where the sulfur and oxygen isotopic compositions increase in the residual sulfate pool at a constant ratio (see also 'Trend b' in Fig. 2b). The first-order Taylor series expansion around the point ($\delta^{34}S_{SO_4}$, $\delta^{18}O_{SO_4}$) = ($\delta^{34}S_{SO_4(0)}$, $\delta^{18}O_{SO_4(0)}$) of

Eq. (5) provides information about the behavior of $\delta^{18}O_{SO_4}$ vs. $\delta^{34}S_{SO_4}$ at the onset of the BSR and is equal to:

$$\delta^{18}O_{SO_{4(t)}} = \delta^{18}O_{SO_{4(0)}} + (\delta^{18}O_{SO_{4(A.E)}} - \delta^{18}O_{SO_{4(0)}}) \cdot \theta_0 \cdot \frac{\delta^{34}S_{SO_{4(t)}} - \delta^{34}S_{SO_{4(0)}}}{\varepsilon^{34}S_{total}} \quad (6)$$

We term this the slope of the apparent linear phase (SALP) in $\delta^{18}O_{SO_4}$ vs. $\delta^{34}S_{SO_4}$ space:

$$SALP = \theta_0 \cdot \frac{\delta^{18}O_{SO_{4(A.E)}} - \delta^{18}O_{SO_{4(0)}}}{\varepsilon^{34}S_{total}} \quad (7)$$

This equation suggests that the SALP is directly proportional to θ_0. SALP is also inversely proportional to $\varepsilon^{34}S_{total}$.

(1) *Apparent equilibrium phase*. This phase refers to the later phase of BSR where the oxygen isotope composition of the residual sulfate pool reaches a constant value, while the sulfur isotope composition continues to increase (Wortmann et al., 2007 and Turchyn et al., 2010, see also 'Trend b' in Fig. 2b). Here we modified the term for the apparent equilibrium of $\delta^{18}O_{SO_4}$ that was given by Turchyn et al. (2010), and also presented in Eq. (4). This is because the term that was formulated by Turchyn et al. (2010) assumed that the uptake of sulfate into the cell (step 1) involves no kinetic isotope effect for oxygen, although a kinetic isotope effect for sulfur does exist. If there is a kinetic oxygen isotope fractionation during sulfate uptake, (step 1) and during the reduction of APS to sulfite (step 3), then the apparent equilibrium value of $\delta^{18}O_{SO_4}$ ($\delta^{18}O_{SO_{4(A.E)}}$) is given by (see Appendix B for the full derivation):

$$\delta^{18}O_{SO_{4(A.E)}} = \delta^{18}O_{H_2O} + \varepsilon^{18}O_{exchange} + \frac{\varepsilon^{18}O_{f\_1}}{X_1 \cdot X_3} + \frac{\varepsilon^{18}O_{f\_3}}{X_3} \quad (8)$$

Previous studies have used plots of θ_0 vs. $\varepsilon^{34}S_{total}$ to investigate the mechanism of BSR (Turchyn et al., 2010; Brunner et al., 2012). There is an ambiguity with calculating X_1 and X_2 separately using isotopes since there is understood to be no isotopic fractionation at step 2 (e.g. Rees (1973)). Therefore, if we consider the two main intracellular branching points in the schematic in Fig. 1 (similar to Farquhar et al., 2003; Canfield et al., 2006), we can rethink the reaction schematic in Fig. 1 without the APS intermediate as shown in Fig. 3 (another way to work around this ambiguity is by merging steps 1 and 2 into one single step. This choice would also have no impact on the calculation). In this case, θ_0 is equal to (after Brunner et al., 2012):

$$\theta_0 = \frac{X_1 \cdot X_3}{1 - X_1 \cdot X_3} \quad (9)$$

and the $\varepsilon^{34}S_{total}$ according to Rees (1973) is:

$$\varepsilon^{34}S_{total} = -3 + 25 \cdot X_1 + 25 \cdot X_1 \cdot X_3 \quad (10)$$

We acknowledge the fact that recent studies have found sulfur fractionation much higher than 47‰ (e.g. Habicht and Canfield, 1996; Wortmann et al., 2001; Sim et al., 2011a), which is the maximum fractionation that Eq. (10) predicts. This however, can be solved by adding another branching point and not by simply adding the additional fractionation (about 50‰) to step 3 (Brunner et al., 2012). Since it is not clear what are the exact environmental constraints activate the trithionite pathway, at this point, we stick to the traditional pathway and will examine if it can simulate pore fluid $\delta^{18}O_{SO_4}$ and $\delta^{34}S_{SO_4}$.

These equations provide unique solutions for X_1 (the ratio between sulfate being brought in and out of the cell) and X_3 (the ratio between the forward and backward fluxes at step 3). Because θ_0 and $\varepsilon^{34}S_{total}$ can be written in terms of X_1 and X_3, we can calculate $\varepsilon^{34}S_{total}$ and θ_0 for a range of X_1 and X_3 values and contour them on a θ_0 vs. $\varepsilon^{34}S_{total}$ diagram (Fig. 4). This allows us to depict variations in θ_0 vs. $\varepsilon^{34}S_{total}$ in terms of variations in X_1 and X_3 during BSR. X_1 provides nearly vertical contours in θ_0 vs. $\varepsilon^{34}S_{total}$ space, suggesting that variations in the flux at step 1 are the main cause for changes in the expressed sulfur isotope fractionation ($\varepsilon^{34}S_{total}$), especially at lower values of X_3. On the other hand, X_3 contours horizontally, suggesting that changes in this step cause the most significant impact on θ_0. The plot of θ_0 vs. $\varepsilon^{34}S_{total}$ (Fig. 4) has similarities with the theoretical $\lambda_{H_2S\text{-}SO_4}$ vs. $1000\ln(r^{34}{}_{H_2S}/r^{34}{}_{SO_4})$ diagram designed by Farquhar et al. (2003). Both diagrams are based on multiple reaction pathways for sulfate within the bacterial cell. The rate and direction of these reactions control the sulfur and oxygen isotope evolution of sulfate. We can use the θ_0 vs. $\varepsilon^{34}S_{total}$ to interpret the mechanism of BSR for our data and previously published work. An extension would be to investigate the mechanism using a $\lambda_{H_2S\text{-}SO_4}$ vs. $1000\ln(r^{34}{}_{H_2S}/r^{34}{}_{SO_4})$ diagram as more $r^{33}{}_{SO_4}$ data becomes available.

2.2. Testing the proposed model

Our changes to the existing models of bacterial sulfate reduction now allow it to be applied to a wider range of timescales and parameter space observed in natural environments. We will apply it now to a pure culture study to show its applicability. Mangalo et al. (2008) carried out five pure culture experiments, with *Desulfovibrio desulfuricans* and ^{18}O enriched water (about 700‰) and varied the nitrite concentration. Nitrite is an inhibitor for the enzyme dissimilatory sulfite reductase used in Step 4 (Greene et al., 2003). Increased nitrite concentrations should, therefore, lead to less reduction of sulfite to sulfide and potentially more recycling of sulfite back to sulfate (Fig. 1). In other words, the higher the nitrite concentration, the higher the backward flux at step 3 (the reoxidation of sulfite to APS), and θ_0 should increase.

The $\delta^{18}O_{H_2O}$ in these experiments was strongly enriched in ^{18}O (700‰ Mangalo et al., 2008). This allows us to investigate the contribution of each step during BSR to the evolution of $\delta^{18}O_{SO_4}$ vs. $\delta^{34}S_{SO_4}$, since it significantly reduces

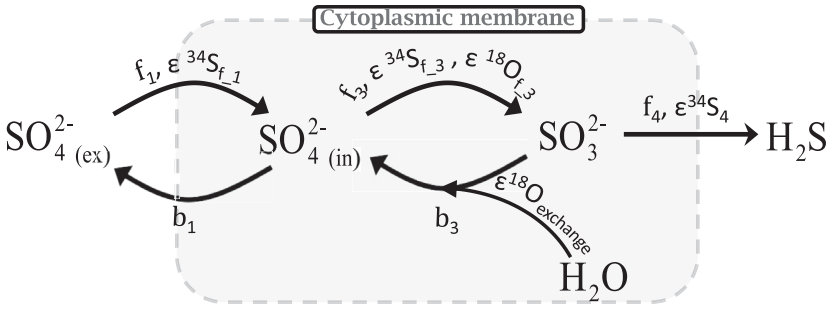

Fig. 3. Simplification of the bacterial sulfate reduction pathway shown in Fig. 1 without the APS intermediate, and considering two branching points (Farquhar et al., 2003; Canfield et al., 2006).

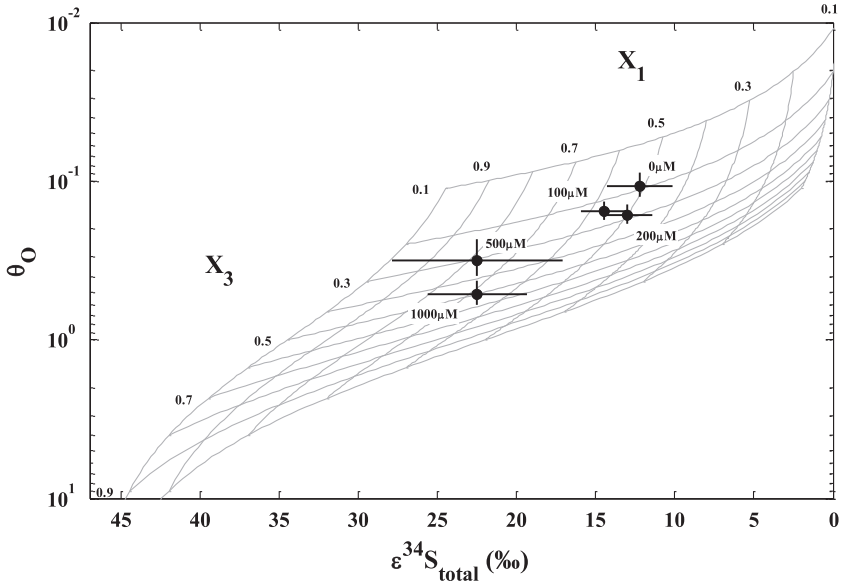

Fig. 4. θ_0 vs. $\varepsilon^{34}S_{total}$ diagram as calculated by Eqs. (9) and (10). The gray circles are calculated from Mangalo et al. (2008). The numbers are the values of nitrate concentrations in the corresponding experiment. Error bars are calculated by the error between two parallel growth experiments.

the uncertainty on the expected $\delta^{18}O_{SO_4(A.E)}$. We calculated the θ_0 for each experiment in Mangalo et al. (2008) using Eq. (7). The SALP was obtained from a linear regression of $\delta^{18}O_{SO_4}$ vs. $\delta^{34}S_{SO_4}$ presented in Mangalo et al. (2008) and the sulfur isotope fractionation ($\varepsilon^{34}S_{total}$) was taken from their calculation. The Mangalo et al. (2008) data is presented on the θ_0 vs. $\varepsilon^{34}S_{total}$ diagram (Fig. 4).

By changing the nitrite concentration, Mangalo et al. (2008) were indeed able to affect the value of X_3, the ratio of the forward and backward fluxes at step 3. Our analysis shows that the SALP of each experiment shows a strong correlation to the nitrite concentration (Fig. 5a) and with X_3 (Fig. 5b) ($R^2 = 0.9987$). However, it seems that there is a poor correlation between X_1 and the SALP (Fig. 5b) ($R^2 = 0.3002$). This suggests that X_3 is directly responding to nitrite concentration, confirming that nitrite was inhibiting sulfite reduction at step 4 (f_4 decreases) and resulting in more sulfite being reoxidized to APS (b_3 increases). In addition, these results suggest that X_3 is the dominant factor controlling the SALP in these experiments.

Analysis of the Mangalo et al. (2008) data shows that the model may help calculate X_1 and X_3 during BSR in pure culture. Application to the natural environment still requires consideration of how the expression of the mechanism of BSR will be seen within pore fluid profiles, which we will consider in Section 5. First we will present our analytical methods and results.

3. METHODS

3.1. Study sites

We present pore fluid profiles from seven new sites (see Map, Fig. 6). The first two sites, Y1 and Y2 are in the Yarqon Stream estuary, Israel (Fig. 6b), with a water depth of ~2 m. Cores were taken using a gravity corer, total core lengths were 29 and 9 cm, for Y1 and Y2 respectively. The Yarqon estuary sediments have a very high organic carbon content of 2.5% and are in contact with brackish

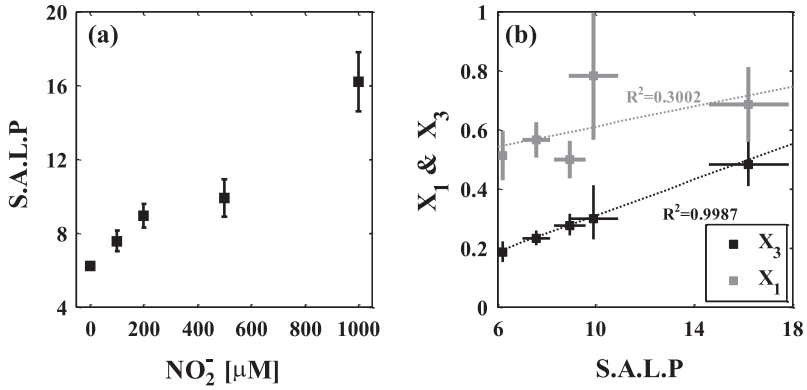

Fig. 5. The SALP vs. nitrite concentration (a) and X_1 (grey squares) and X_3 (black squares) vs. the SALP from pure culture *D. desulfuricans* (modified after Mangalo et al., 2008) (b). Error bars for the SALP are calculated by the difference between two parallel growth experiments, and the error bars for X_1 and X_3 indicate the maximum and minimum values calculated using Eqs. (9) and (10). The lines in panel (b) are the best-fit curves of the linear regression.

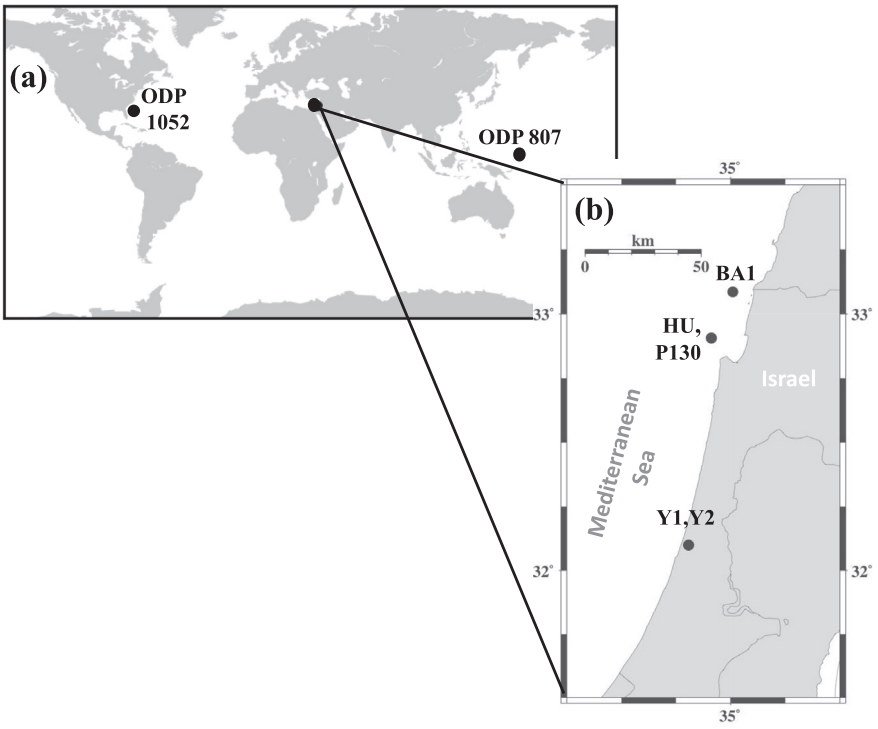

Fig. 6. Maps of the study area in a map of the world (a), and a map of the Eastern Mediterranean region (b). The dots and the corresponding labels indicate the site locations and names, respectively.

bottom waters (~19 g Cl l^{-1}), due to seawater penetration into the estuary.

Cores were collected at three sites on the shallow shelf of the Eastern Mediterranean Sea off the Israeli coast; Sites HU, 130 and BA1 (Fig. 6b), with water depths of 66, 58 and 693 m, respectively. Total core lengths for the three sites were 234, 254 and 30 cm, respectively. The sediment from site BA1 was collected using a box corer, while a piston corer was used for sites 130 and HU. The organic carbon content at these sites ranges from ~0.5–1.0%. Finally, pore fluid profiles are also presented from advanced piston cores collected by the Ocean Drilling Program (ODP) at ODP Sites 1052 and 807. Site 1052 (Leg 171B), is located on Blake Nose (NW Atlantic Ocean) at a water depth of 1345 m, with a total sediment penetration of 684.8 m (60.2% recovery). Site 807 (Leg 130) (Fig. 6a), is located on the Ontong-Java Plateau (tropical NW Pacific) at a water depth of 2805 m with a total sediment penetration of 822.9 m (87.1% recovery). The organic carbon content at Site 1052 it is below 1%, while at Site 807 ranges between 0.02% and 0.6%.

3.2. Analytical methods

The samples from the Yarqon estuary and the Eastern Mediterranean sites were processed at Ben Gurion University of the Negev, Israel, usually on the same day as coring. The cores were split into 1 cm slices under an argon purge. The pore fluids were extracted from each cm slice by centrifuging under an argon atmosphere to avoid oxygen contamination. The samples were acidified and purged with argon to remove sulfides and prevent their oxidation to sulfate. The sulfate concentration in the pore fluids from the Yarqon estuary was measured by high performance liquid chromatography (HPLC, Dionex DX500) with a precision of 3%. The total sulfur (assumed to be only sulfate) concentrations from the Eastern Mediterranean were measured by inductivity coupled plasma-atomic emission (ICP-AES, P-E optima 3300) with a precision of 2%.

The ODP sediments were handled using standard shipboard procedures. Sulfate concentrations of the pore fluids from the ODP Sites were measured by Dionex ion chromatograph onboard the ship. Pore fluid sulfate from the Yarqon estuary, the Eastern Mediterranean and the ODP sites were then precipitated as barium sulfate (barite) by adding a saturated barium chloride solution. The barite was subsequently rinsed with acid and deionized water and set to dry in a 50 °C oven.

The sulfur and oxygen isotope composition of the pore fluid sulfate were analyzed in the Godwin Laboratory at the University of Cambridge. The barite precipitate was pyrolyzed at 1450 °C in a Temperature Conversion Element Analyzer (TC/EA), and the resulting carbon monoxide (CO) was measured by continuous flow GS-IRMS (Delta V Plus) for its $\delta^{18}O_{SO_4}$. For the $\delta^{34}S_{SO_4}$ analysis the barite was combusted at 1030 °C in a Flash Element Analyzer (EA), and resulting sulfur dioxide (SO_2) was measured by continuous flow GS-IRMS (Thermo, Delta V Plus). Samples for $\delta^{18}O_{SO_4}$ were run in replicate and the standard deviation of these replicate analyses was used ($< 0.4‰$). The error for $\delta^{34}S_{SO_4}$ was determined using the standard deviation of the standard NBS 127 at the beginning and the end of each run ($\sim 0.2‰$). Samples for both $\delta^{18}O_{SO_4}$ and $\delta^{34}S_{SO_4}$ were corrected to NBS 127 (8.6‰ for $\delta^{18}O_{SO_4}$ and 20.3‰ for $\delta^{34}S_{SO_4}$). A second laboratory derived barite standard was run for $\delta^{18}O_{SO_4}$ (16‰) to correct for linear changes during continuous flow over a range of $\delta^{18}O_{SO_4}$ values and to map our measurements more accurately in isotope space. Since the bulk of our $\delta^{18}O_{SO_4}$ data falls between 8‰ and 21‰, these standards were appropriate for the isotope range of interest.

4. FIELD RESULTS

The pore fluid sulfate concentrations and oxygen and sulfur isotope compositions for the seven new sites are shown in Fig. 7. The cores from the Yarqon estuary (Y1, 29 cm and Y2, 9 cm, Fig. 7a–c) are similar and show almost total depletion in pore fluid sulfate (site Y1, Fig. 7c). As sulfate concentrations decrease, both the $\delta^{18}O_{SO_4}$ and $\delta^{34}S_{SO_4}$ of the sulfate increase. At the greater depths, $\delta^{34}S_{SO_4}$ continues to increase, while $\delta^{18}O_{SO_4}$ reaches a constant value of 23–24‰ (site Y1 Fig. 7c).

The results from sites BA1 (30 cm) HU (234 cm) and P130 (254 cm) are shown in Fig. 7e–f. There is a maximum of 40% consumption of sulfate, within the upper 234 cm at Site HU, and within 250 cm at Site P130. Both the $\delta^{18}O_{SO_4}$ and $\delta^{34}S_{SO_4}$ increase with depth at both sites: the $\delta^{34}S_{SO_4}$ increases to 30.3‰ and the $\delta^{18}O_{SO_4}$ increases to 19.0‰ at site HU, while at site P130 the $\delta^{34}S_{SO_4}$ increases to 38.8‰ and the $\delta^{18}O_{SO_4}$ increases to 24.0‰. At site BA1, $\delta^{18}O_{SO_4}$ and $\delta^{34}S_{SO_4}$ both increase while the pore fluid sulfate concentration decreases (Fig. 7d–f).

In ODP Sites 807 and 1052, pore fluid sulfate concentrations remain constant in the upper 30 m, and then decrease over the next ~200 m by 25% and 50%, respectively (Fig. 7g–i). At both Sites, the $\delta^{34}S_{SO_4}$ increases with decreasing sulfate concentrations, to values of 28–29‰ at ~300 m. The $\delta^{18}O_{SO_4}$ also increases to 22–23‰ at both Sites.

5. DISCUSSION

5.1. Applying our time-dependent closed system model to pore fluid profiles

In this section we discuss the use of our model of BSR (Sections 2.1 and 2.2) to understand what controls the relative evolution of $\delta^{18}O_{SO_4}$ vs. $\delta^{34}S_{SO_4}$ in the natural environment. Applying what is effectively a "closed system" model to an "open system" (environmental pore fluids) requires understanding the physical parameters that control each of the sulfate species concentrations (in our case $^{34}S^{16}O_4^{2-}$, $^{32}S\ ^{18}O^{16}O_3^{2-}$ and $^{32}S^{16}O_4^{2-}$) within the fluids in the sediment column (Jørgensen, 1979; Chernyavsky and Wortmann, 2007; Donahue et al., 2008;Wortmann and Chernyavsky, 2011).

In this study we utilize SALP, that is the relative change of $\delta^{18}O_{SO_4}$ vs. $\delta^{34}S_{SO_4}$, rather than the $\delta^{18}O_{SO_4}$ value during apparent equilibrium although both hold information about the mechanism of the BSR (see Eqs. (7) and (8)). Focusing on SALP enables investigating the mechanism of BSR from sites that were not cored deep enough to observe apparent equilibrium (e.g. Mediterranean Sea sediments from this study, Fig. 7d–f). Also, it is not clear whether the $\delta^{18}O_{SO_4}$ really reaches equilibrium values at some sites (e.g. the ODP Sites, Fig. 7g–i).

The outstanding question is how can we apply SALP as observed in the relative evolution of the $\delta^{18}O_{SO_4}$ and $\delta^{34}S_{SO_4}$ in the pore fluids to the model for the biochemical steps during BSR as derived for pure cultures? How do you bridge the gap between the "closed system" equations and the application to the "open system"? To explore this, we will briefly explore how SALP changes between closed and open systems in two extreme cases: (a) Deep-sea temperature (2 °C), low sedimentation rate (10^{-3} cm year^{-1}) and slow net sulfate reduction rate (low as 10^{-12} mol cm^{-3} year^{-1}), typical of deep-sea environments versus (b) Surface temperature (25 °C), high sedimentation rate (10^{-1} cm year^{-1}) and high net sulfate reduction rate (5×10^{-4} mol cm^{-3} year^{-1}) conditions similar to shallow marginal-marine

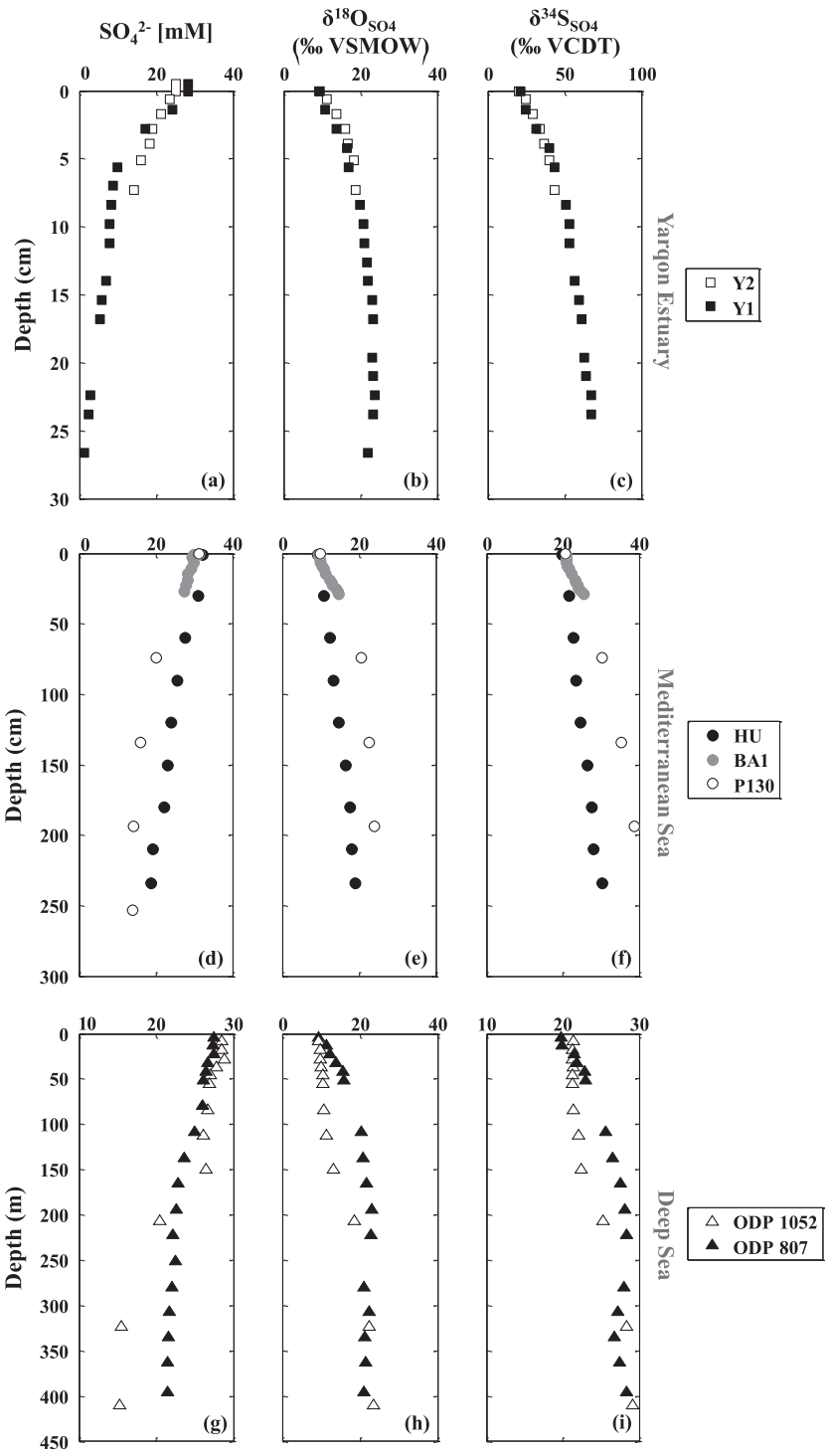

Fig. 7. Pore fluid profiles in the Yarqon estuary at sites Y1 (filled symbols) and Y2 (open symbols) of SO_4^{2-} (a), $\delta^{18}O_{SO_4}$ (b), and $\delta^{34}S_{SO_4}$ (c). Pore fluid profiles in the Mediterranean Sea at sites HU (filled symbols), BA1 (gray symbols) and P130 (open symbols) of SO_4^{2-} (d), $\delta^{18}O_{SO_4}$ (e) and $\delta^{34}S_{SO_4}$ (f). Pore fluid profiles in ODP Sites 807 (filled symbols) and 1052 (open symbols) of SO_4^{2-} (g), $\delta^{18}O_{SO_4}$ (h) and $\delta^{34}S_{SO_4}$ (i).

environments. In each case we have calculated the "closed system" solution for a given mechanism, or intracellular fluxes during BSR, and then separately calculated the "open system" for the same mechanism give the natural conditions described above. For the entire model description see Appendix C.

Fig. 8 presents the calculated open system versus closed system SALP for the two extreme environments, as function of the change in X_3 (where X_1 is fixed and equal to 0.99). It can be seen that in applying the close system solution to the open system can lead to underestimation of as much as 10% in the value of X_3 (For changes in X_1, the

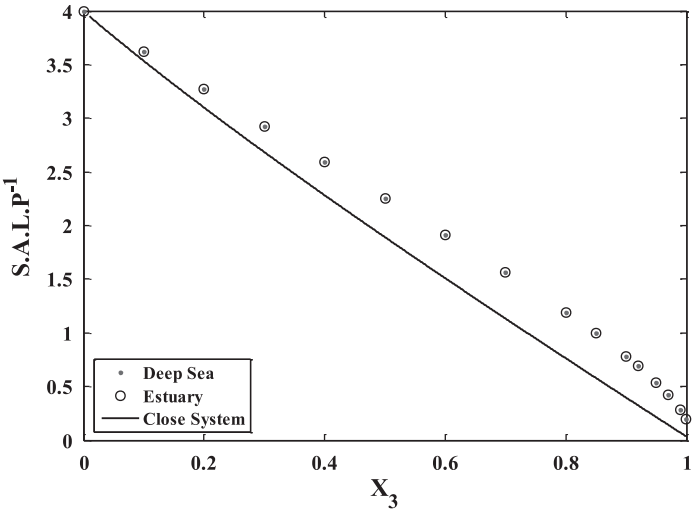

Fig. 8. The SALP and function of X_3 (where X_1 is fixed and close to unity) for three different scenarios: Closed system (according to Eq. (11)), simulation of typical deep-sea sediment and simulation of typical estuary sediment.

misestimate will be similar in magnitude). Although there are vastly different physical parameters between these two synthetic sites, the resulting calculated SALPs are not significantly different. This similarity in calculated SALP is because the main difference moving to an open system from a closed system is the change the relative diffusion flux of any of the isotopologues. We conclude that we can read the SALP from $\delta^{18}O_{SO_4}$ and $\delta^{34}S_{SO_4}$ pore fluid profiles (e.g. Fig. 2) and apply our closed system model to understand the mechanism, with the caveat that we have error bars on our resulting interpretation.

5.2. What controls the relative evolution of $\delta^{18}O_{SO_4}$ vs. $\delta^{34}S_{SO_4}$ in marine sediments during BSR

It has been suggested that in the natural environment as well as in pore fluids, the relative evolution of $\delta^{18}O_{SO_4}$ vs. $\delta^{34}S_{SO_4}$ (SALP) is connected to the overall sulfate reduction rate (Böttcher et al., 1998, 1999; Aharon and Fu, 2000; Brunner et al., 2005). We further suspect that the relative evolution provides information about the mechanism, or individual intracellular steps, during BSR. A plot of our data in $\delta^{18}O_{SO_4}$ vs. $\delta^{34}S_{SO_4}$ space displays a close-to-linear relationship between $\delta^{18}O_{SO_4}$ and $\delta^{34}S_{SO_4}$ (Fig. 9). The slope, however, varies greatly among the different sites (Fig. 9). In general, the sites from the shallower estuary environments have a more moderate slope (0.35–0.44), meaning the sulfur isotopes increase rapidly relative to the oxygen isotopes, while the shallow marine sediments have steeper slopes (0.99–1.1), and the deep-sea sediments have the steepest slopes (1.7 and 1.4, respectively). The ODP Sites thus show the fastest increase in the $\delta^{18}O_{SO_4}$ relative to the $\delta^{34}S_{SO_4}$ compared with the shallower sites. The changes in the slope among the different sites correlates with the depth dependent sulfate concentration profiles, where the higher the rate of change in the sulfate concentration with depth below the sediment–water interface, the lower the slope, or the more quickly the sulfur isotopes evolve relative to the oxygen isotopes. Site P130 (Mediterranean) is the exception and does not show a linear relationship between $\delta^{18}O_{SO_4}$ and $\delta^{34}S_{SO_4}$, likely due to poor sampling resolution.

Previous studies have shown a similar initial linear relationship between $\delta^{18}O_{SO_4}$ and $\delta^{34}S_{SO_4}$, with the slope ranging between 1:1.4 (=0.71 compared to our cross plots, Aharon and Fu, 2000) to 1:4.4 (=0.22, Mandernack et al., 2003). Our data (Fig. 9) displays a wider variation in slope than previously reported, as anticipated in this study. Most authors have attributed the linear evolution of sulfur versus oxygen isotopes in sulfate during BSR to a fully kinetic isotope effect in a closed system under 'Rayleigh distillation', neglecting equilibrium oxygen isotope fractionation. The SALP, however, includes the equilibrium oxygen isotope effect during initial BSR prior to reaching apparent equilibrium.

We calculated the net sulfate reduction rate (nSRR) from each site from a curve fit of the sulfate concentration profiles in the pore fluids using the general diagenetic equation (Berner, 1980). As sulfate from the ocean diffuses into the sediments to be reduced to sulfide, the length, or depth, scale over which sulfate concentrations decrease relates to the overall rate of sulfate reduction. We assume the sulfate concentration is in steady state (this is based on the fact that the age of the sediments at all the sites in this study is much higher than the characteristic timescale of diffusion) and no advection. However, we acknowledge that these assumptions may be wrong in some of our sites. To augment our data we also present nSRR from pore fluids profiles in previously published studies, where sulfate concentrations and sulfur and oxygen isotopes in sulfate were published. This allows us to scale our results and model to an even wider range of environments than those we directly measured. Table EA.1 in the Electronic Annex summarizes data from the literature and the location for each site.

In this larger dataset, the inverse of the slope between $\delta^{18}O_{SO_4}$ vs. $\delta^{34}S_{SO_4}$ is positively correlated with the logarithm of the nSRR (Fig. 10). This observation confirms

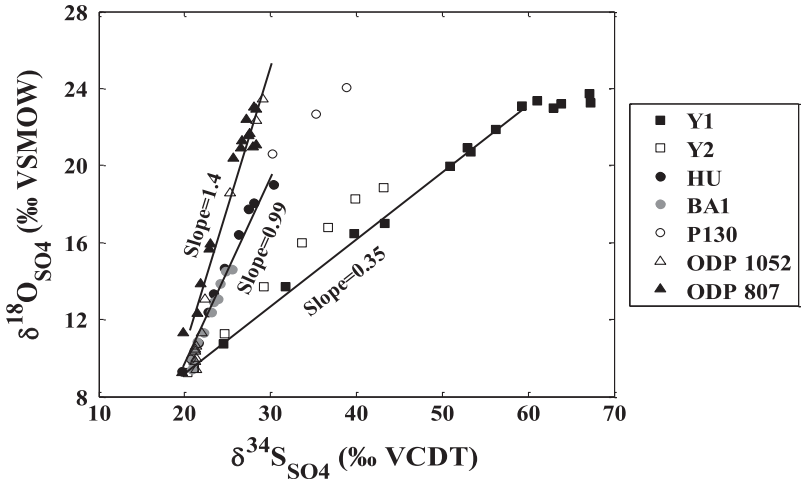

Fig. 9. $\delta^{18}O_{SO_4}$ vs. $\delta^{34}S_{SO_4}$ data in pore fluid sulfate of all studied sites. The lines are the linear regressions for Sites Y1, HU and 807.

the hypothesis of Böttcher et al. (1998, 1999), who suggested that increases in overall nSRR, would result in decreases in the expressed sulfur and oxygen isotope fractionation, and thus the shape of $\delta^{18}O_{SO_4}$ vs. $\delta^{34}S_{SO_4}$ in sedimentary pore fluids.

5.3. The mechanism of BSR in marine sediments

Our compilation from pore fluids in a diverse range of natural environments suggests a correlation between the SALP and the nSRR (Fig. 10). This association may provide further understanding about the mechanism of BSR in the natural environment. Combining the first order approximation for the SALP (Eq. (7)) together with Eqs. (8)–(10) yields:

$$\mathrm{SALP} = \frac{1}{1 - X_1 \cdot X_3} \cdot \frac{\frac{\varepsilon^{18}O_{f\_1}}{X_1 \cdot X_3} + \frac{\varepsilon^{18}O_{f\_3}}{X_1} + \delta^{18}O_{H_2O} + \varepsilon^{18}O_{\mathrm{exchange}} - \delta^{18}O_{SO_{4(0)}}}{\frac{\varepsilon^{34}S_{f\_1}}{X_1 \cdot X_3} + \frac{\varepsilon^{34}S_{f\_3}}{X_1} + \varepsilon^{34}S_{f\_4}} \tag{11}$$

Eq. (11) shows that the SALP is a function of both X_1 and X_3 and does not depend on one more than the other. Hence, a change in the SALP does not necessarily tell us which one of the above (X_1 or X_3) plays more important role in the relative evolution of $\delta^{18}O_{SO_4}$ vs. $\delta^{34}S_{SO_4}$.

In order to address the question of the relative importance of X_1 vs. X_3 in the natural environment, we solved Eq. (5) for three different cases:

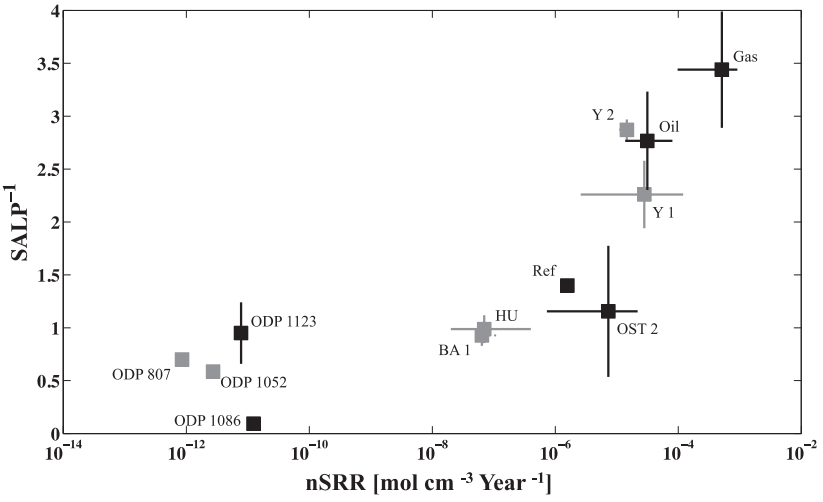

Fig. 10. The slope of $\delta^{34}S_{SO_4}$ vs. $\delta^{18}O_{SO_4}$ in the apparent linear phase of BSR vs. the average nSRR, as deduced from our data and worldwide pore fluid profiles. Data are presented from this study (open circles) and from other references (close circles). The labels of each point indicate the site's name (the coresponding references for each site are given in Table EA.1 in the Electronic Annex).

(1) X_1 varies and X_3 is fixed (close to unity) – that is, the flow of sulfate in and out of the cell varies but the recycling of sulfite is fixed such that nearly all the sulfite is reoxidized back to the internal sulfate pool.
(2) X_3 varies and X_1 is fixed (close to unity) – that is the percentage of the recycling of the sulfite varied but the flow of sulfate in and out of the cell is fixed such that nearly all the sulfate that is brought into the cell exit the cell eventually.
(3) Both X_1 and X_3 vary simultaneously.

The initial condition for this calculation is set by the isotopic composition of surface seawater sulfate (roughly 10‰ and 20‰ for oxygen and sulfur isotopes, respectively). The kinetic sulfur isotope effect for each step is similar to the values previously described (Rees, 1973). The kinetic oxygen isotope fractionation is taken to be 1/4 of the fractionation of the sulfur isotope (Mizutani and Rafter, 1969). The total equilibrium oxygen isotope fractionation between sulfite and the AMP-sulfite complex and ambient water is taken as 17‰, which produces an apparent equilibrium of about 22‰ in the case where X_1 and X_3 equal 1 (Eq. (8)). As discussed in the introduction, it is enigmatic what impact temperature has on the $\delta^{18}O_{SO_4(A.E)}$. We therefore consider equilibrium oxygen isotope fractionation between sulfite and the AMP-sulfite complex and ambient water as constant among the different environments (Eq. (8)). The results from this calculation are shown in Fig. 11a–c, with the measured data included for comparison in Fig. 11d.

The model solution for $\delta^{18}O_{SO_4}$ and $\delta^{34}S_{SO_4}$, when varying X_3 only (Fig. 11b) fits the general behavior of pore fluid sulfur and oxygen isotopes (Fig. 11d) highlighting the importance of X_3 on the relative evolution of $\delta^{18}O_{SO_4}$ and $\delta^{34}S_{SO_4}$ in the natural environment. The best-fit curves for the pore fluids in this study are presented as the solid lines in Fig. 11d. This calculation suggests values for X_1 near unity (ranging between 0.96 and 0.99 – indicating up to 99% of the sulfate brought into the cell is ultimately recycled back out the cell). However, we suggest that this kind of forward modeling is not accurate enough to estimate the real values for X_1 and X_3 in natural environments due to the uncertainty with the values in our model as well as the application of a closed system model to pore fluids. Therefore, changes in X_1 may be more important to the relative evolution of $\delta^{18}O_{SO_4}$ vs. $\delta^{34}S_{SO_4}$ than our calculation suggest. In addition, our solution is valid only if BSR is the only process that affects sulfur and oxygen isotopes in sulfate – which may not be the case. Other subsurface processes can also affect this evolution, such as pyrite oxidation (e.g. Balci et al., 2007; Brunner et al., 2008; Heidel and Tichomirowa, 2011; Kohl and Bao, 2011) or sulfur disproportionation (Cypionka et al., 1998; Böttcher et al., 2001, 2005; Böttcher and Thamdrup, 2001).

Although most of the sites with $\delta^{18}O_{SO_4}$ and $\delta^{34}S_{SO_4}$ data seem to fit our model, our closed system model cannot replicate scenarios where the apparent equilibrium values are relatively high (26–30‰) together with a steep SALP (higher than ~1) in the uppermost sediments. As a result, by applying the closed system model, we cannot simulate data from Sites like ODP Site 1225 (Blake et al., 2006; Böttcher et al., 2006) and ODP Site 1130 (Wortmann et al., 2007). We suggest that this may be an artifact of the uncertainty in the values of the oxygen isotopic fractionation during various intracellular processes or erroneous model assumptions; these include the possible importance of temperature on oxygen exchange with ambient water (e.g. Fritz et al., 1989; Zeebe, 2010) or our assumption that this isotope exchange is complete, which it may not be (Brunner et al., 2012). The high sulfur isotope fractionation (>40‰) at these sites is consistent with the occurrence other complicating factors, such as activation of the trithionite pathway or subsurface sulfur disproportionation (Canfield and Thamdrup, 1994; Brunner and Bernasconi, 2005) that may skew the SALP, but which our model does not take into account.

5.4. The role of sulfite reoxidation in marine sediments

Our model suggests that X_3 varies between 0.4 and ~1 in the natural environments we studied (Fig. 11), and is inversely correlated with nSRR. This hints that the reduction of sulfite to sulfide (Step 4) is connected to nSRR in marine sediments and may be the "bottleneck reaction", or significant branching point, for overall BSR. The faster the reduction of sulfite to sulfide, and therefore faster overall SRR, less sulfite is being reoxidaized back to the outer sulfate pool. But what environmental or natural parameters control the functioning of this bottleneck?

We attribute secondary importance to pressure differences (also Vossmeyer et al., 2012) among natural environments, since we found similar isotope behavior among sites that varied in water depth (i.e. pressure). Similar to Kaplan and Rittenberg (1964) and Bradley et al. (2011), we speculate that one of the major environmental factors that could impact the different behavior of the communities of sulfate reducing bacteria might be related to the supply of the electron from the electron donor or carbon source. It has been shown that the nature and concentration of different electron donors is connected to the dynamics of each step during BSR (Brüchert, 2004; Sim et al., 2011b), and the overall nSRR (e.g. Westrich and Berner, 1984). Our data suggest that the higher the nSRR, the lower the sulfite reoxidation (over step 4, sulfite reduction). This recycling of sulfite likely plays a critical role during BSR in marine sediments. One possibility is that where the availability of the electron donor is low (less organic matter availability), such as in deep marine sediments, sulfate reducing bacteria might maintain high intracellular concentrations of sulfite, which is manifest geochemically as the rapid change in $\delta^{18}O_{SO_4}$ relative to the slower change in $\delta^{34}S_{SO_4}$. This could be contrasted with environments where there is high organic matter availability (for example marginal and shallow marine environments) where significant concentrations of intracellular sulfite would be unnecessary. Although highly speculative, we suggest there is a relationship between the concentration of intracellular sulfite and the availability of the electron donor in the natural environment. Our data suggests that this relationship may impact the relative fluxes within the bacterial sulfate reducing community.

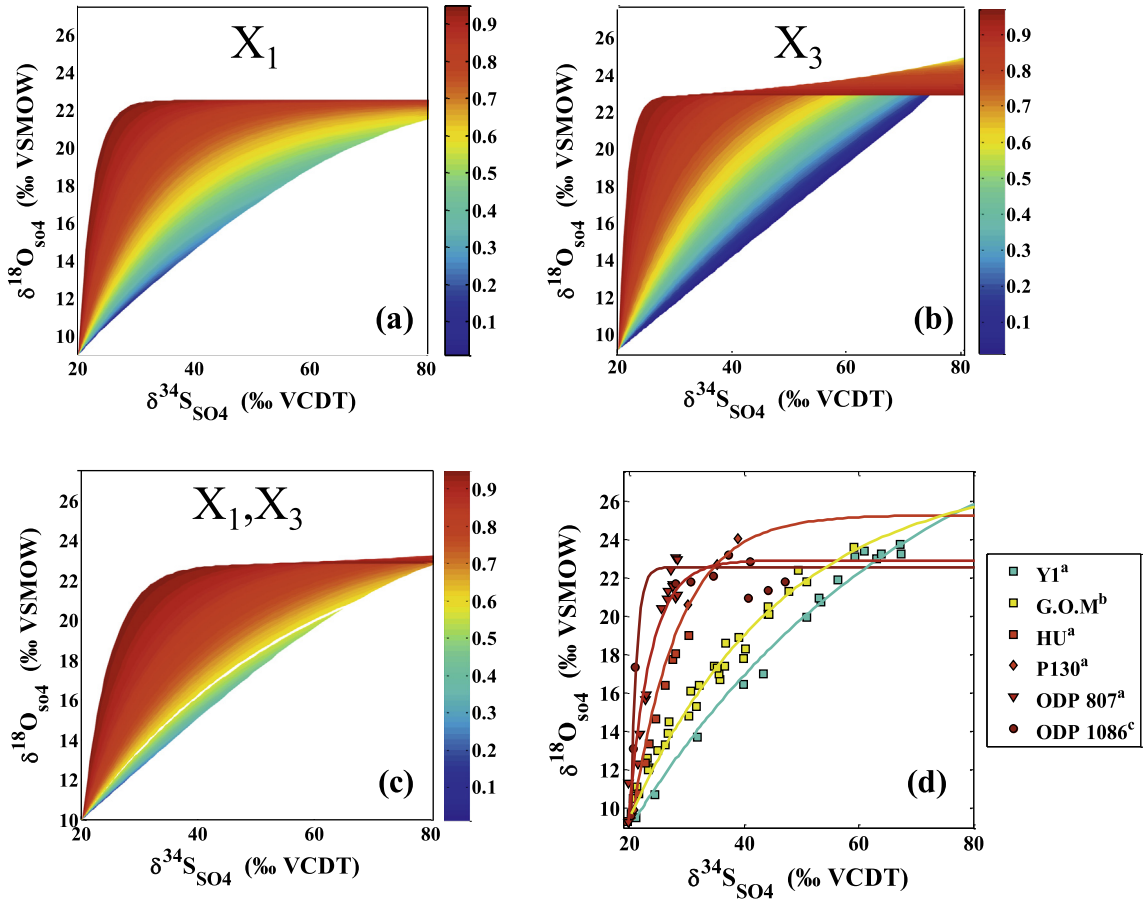

Fig. 11. Schematic $\delta^{18}O_{SO_4}$ vs. $\delta^{34}S_{SO_4}$ plots, where X_1 varies and X_3 is fixed (close to unity) (a), X_3 varies and X_1 is fixed (close to unity) (b), both X_1 and X_3 vary simultaneously (c) and $\delta^{18}O_{SO_4}$ vs. $\delta^{34}S_{SO_4}$ data of pore fluid sulfate, the solid lines are the best-fit solution for X_1 and X_3 for each site as the color of the line is corresponding to the calculated X_3 value (d). [(a)]This study, [(b)]Aharon and Fu (2000), and [(c)]Turchyn et al. (2006). (For interpretation of the references to color in this figure legend, the reader is referred to the web version of this article.)

Although this paper deals specifically with BSR in the marine environment, it is likely that our results are applicable to BSR in other systems including freshwater and groundwater systems. In these environments the hydrology is much more poorly constrained and the effects of advection and dispersion must be considered (Knöller et al., 2007). While we have taken the first steps towards expanding the applicability of this isotope approach to resolving mechanism, the next logical steps would be to extend the approach to the terrestrial environment where BSR can play a critical role in water quality.

6. SUMMARY AND CONCLUSIONS

In this study we presented pore fluid measurements of $\delta^{34}S_{SO_4}$ and $\delta^{18}O_{SO_4}$ from seven new sites spanning a shallow estuary to a deep-sea sediment. These pore fluid profiles exhibited behavior similar to previously published pore fluid profiles; the $\delta^{34}S_{SO_4}$ increases monotonically during bacterial sulfate reduction, while the $\delta^{18}O_{SO_4}$ increased and at some point levels off, when it has reached apparent equilibrium. When we plot the $\delta^{34}S_{SO_4}$ vs $\delta^{18}O_{SO_4}$ in this large range of natural environments we explored the reason behind the change in slope of $\delta^{34}S_{SO_4}$ vs $\delta^{18}O_{SO_4}$. Combining our results with literature data, we demonstrated that the slope of this line correlated to the net sulfate reduction rate, as has been suggested in previous studies. At sites with high sulfate reduction rates, the $\delta^{18}O_{SO_4}$ increases more slowly relative to the $\delta^{34}S_{SO_4}$, where at sites with lower sulfate reduction rates, the $\delta^{18}O_{SO_4}$ increases more quickly relative to the $\delta^{34}S_{SO_4}$. We reformulated the widely used model for the relative evolution of sulfur and oxygen isotopes in sulfate during BSR. We used this new model with our data to explore how the intracellular fluxes impact the evolution of $\delta^{18}O_{SO_4}$ vs. $\delta^{34}S_{SO_4}$ during bacterial sulfate reduction.

Our new data, together with our new model, suggested that the most significant factor controlling the evolution of $\delta^{18}O_{SO_4}$ vs. $\delta^{34}S_{SO_4}$ in the natural environment is the ratio between the fluxes of intracellular sulfite oxidation and APS reduction (X_3). The variation in the ratio and its correlation to the nSRR implies that sulfite reduction may be the bottleneck reaction during BSR. We suggested that this recycling allows sulfate reduction to proceed even when the organic matter availability is low.

ACKNOWLEDGEMENTS

We are grateful to Dr. D. Pargament and P. Rubinzaft from the Yarkon River Authority and to the crew of the R/V Shikmona from the Israel Oceanographic and Limnological Research Institute (IOLR) for their technical support in the field. We are in debt with E. Eliani-Russak from Ben Gurion University of the Negev and with J. Rolfe from the Godwin Laboratory at the University of Cambridge for their technical support in the laboratory. We are thankful to Prof. G. Jiwchar for the use in the HPLC. We would like to thank B. Brunner, U. G. Wortmann and the 3rd anonymous reviewer that dealt with an earlier version of this manuscript, as well as I. Kohl and two anonymous reviewers that, with their comments, helped improve the final version of this manuscript. G. Antler would like to thanks his colleagues from Ben Gurion University A. Russak, N. Avrahamov, M. Adler, I. Bar-Or and E. Levy for assistance at the field and the lab, as well as Dr. M. Tsesarsky, S. Kadmiel ,Dr. R. Novitsky Nof and Y. Tal for helping with coding.

This research was supported by the British Council BIRAX grant BY2/GEO/04, the Israel Science Foundation (#643/12) and NERC grant NE/H011595/1 to AVT.

APPENDIX A. COMPUTING θ_0/ϵ DIAGRAM

First, we consider the following reaction:

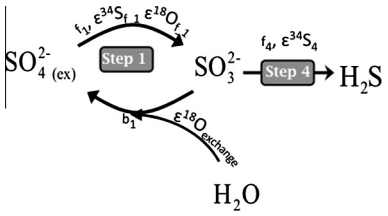

At steady flow the mass balance equation for the sulfate can be written as:

$$\frac{d[SO_4^{2-}]}{dt} = b_1 - f_1 \tag{A.1}$$

And therefore:

$$dt = \frac{d[SO_4^{2-}]}{b_1 - f_1} \tag{A.2}$$

If the oxygen isotopic exchange between the sulfite and the ambient water >> than φ_1, φ_2, φ_3, the isotopic mass balance equation for $\delta^{18}O_{SO_4}$ can be written as:

$$\frac{d([SO_4^{2-}]\cdot\delta^{18}O_{SO_4})}{dt} b_1\cdot(\delta^{18}O_{H_2O}+\varepsilon^{18}O_{exchange}) - f_1 \cdot(\delta^{18}O_{SO_4}-\varepsilon^{18}O_{f\_1}) \tag{A.3}$$

According to the derivative's chain rule and Eq. (A.1):

$$\frac{d([SO_4^{2-}]\cdot\delta^{18}O_{SO_4})}{dt} = [SO_4^{2-}]\cdot\frac{d(\delta^{18}O_{SO_4})}{dt} + \delta^{18}O_{SO_4}\cdot(b_1-f_1) \tag{A.4}$$

And therefore the combination between Eqs. (A.3) and (A.4) gives:

$$[SO_4^{2-}]\cdot\frac{d(\delta^{18}O_{SO_4})}{dt} = b_1\cdot(\delta^{18}O_{H_2O}+\varepsilon^{18}O_{exchange} - \delta^{18}O_{SO_4}) + f_1\cdot(\varepsilon^{18}O_{f\_1}) \tag{A.5}$$

Rearranging Eq. (A.5) results with:

$$\frac{dt}{[SO_4^{2-}]} = \frac{d(\delta^{18}O_{SO_4})}{b_1\cdot(\delta^{18}O_{H_2O}+\varepsilon^{18}O_{exchange}-\delta^{18}O_{SO_4})+f_1\cdot(\varepsilon^{18}O_{f\_1})} \tag{A.6}$$

The combination between Eqs. (A.6) and (A.2) yields:

$$\frac{1}{b_1-f_1}\cdot\frac{d[SO_4^{2-}]}{[SO_4^{2-}]} = \frac{d(\delta^{18}O_{SO_4})}{b_1\cdot(\delta^{18}O_{H_2O}+\varepsilon^{18}O_{exchange}-\delta^{18}O_{SO_4})+f_1\cdot(\varepsilon^{18}O_{f\_1})} \tag{A.7}$$

The solution of Eq. (A.7) with the initial conditions of $\delta^{18}O_{SO_{4(0)}}$ and $[SO_4^{2-}]_{(0)}$ at $t = 0$.

$$\ln\left(\frac{b_1\cdot(\delta^{18}O_{H_2O}+\varepsilon^{18}O_{exchange}-\delta^{18}O_{SO_4})+f_1\cdot(\varepsilon^{18}O_{f\_1})}{b_1\cdot(\delta^{18}O_{H_2O}+\varepsilon^{18}O_{exchange}-\delta^{18}O_{SO_{4(0)}})+f_1\cdot(\varepsilon^{18}O_{f\_1})}\right) = \frac{b_1}{b_1-f_1}\cdot\ln\left(\frac{[SO_4^{2-}]}{[SO_4^{2-}]_{(0)}}\right) \tag{A.8}$$

Defining $\frac{b_1}{f_1}\equiv X_1$

$$\ln\left(\frac{\delta^{18}O_{H_2O}+\varepsilon^{18}O_{exchange}-\delta^{18}O_{SO_4}+\frac{1}{X_1}\cdot(\varepsilon^{18}O_{f\_1})}{\delta^{18}O_{H_2O}+\varepsilon^{18}O_{exchange}-\delta^{18}O_{SO_{4(0)}}+\frac{1}{X_1}\cdot(\varepsilon^{18}O_{f\_1})}\right) = -\frac{X_1}{1-X_1}\cdot\ln\left(\frac{[SO_4^{2-}]}{[SO_4^{2-}]_{(0)}}\right) \tag{A.9}$$

According to Turchyn et al. (2010):

$$\delta^{18}O_{SO_{4(A.E)}} = \delta^{18}O_{H2O}+\varepsilon^{18}O_{exchange}+\frac{1}{X_1}\cdot(\varepsilon^{18}O_{f\_1}) \tag{A.10}$$

Embedding Eqs. (A.10) into (A.9):

$$\ln\left(\frac{\delta^{18}O_{SO_{4(A.E)}}-\delta^{18}O_{SO_4}}{\delta^{18}O_{SO_{4(A.E)}}-\delta^{18}O_{SO_{4(0)}}}\right) = -\frac{X_1}{1-X_1}\cdot\ln\left(\frac{[SO_4^{2-}]}{[SO_4^{2-}]_{(0)}}\right) \tag{A.11}$$

and can be written in more general form:

$$\ln\left(\frac{\delta^{18}O_{SO_{4(A.E)}}-\delta^{18}O_{SO_4}}{\delta^{18}O_{SO_{4(A.E)}}-\delta^{18}O_{SO_{4(0)}}}\right) = -\theta_0\cdot\ln\left(\frac{[SO_4^{2-}]}{[SO_4^{2-}]_{(0)}}\right) \tag{A.12}$$

where θ_0 is only a function of the ratio between the backward and forward fluxes.

According to Rayleigh distillation:

$$\frac{\delta^{34}S_{SO_4}-\delta^{34}S_{SO_{4(0)}}}{\varepsilon^{34}S_{total}} = \ln\left(\frac{[SO_4^{2-}]}{[SO_4^{2-}]_{(0)}}\right) \tag{A.13}$$

$$\delta^{18}O_{SO4(t)} = \begin{cases} \frac{\varepsilon^{18}O_{total}}{\varepsilon^{34}S_{total}} \cdot (\delta^{34}S_{SO4(t)} - \delta^{34}S_{SO4(0)}) + \delta^{18}O_{SO4(0)}; & X_1 \cdot X_2 \cdot X_3 = 0 \\ \delta^{18}O_{SO4(A.E)} - \exp\left(-\theta_0 \cdot \frac{\delta^{34}S_{SO4(t)} - \delta^{34}S_{SO4(0)}}{\varepsilon^{34}S_{total}}\right) \cdot (\delta^{18}O_{SO_4(A.E)} - \delta^{18}O_{SO4(0)}); & 0 < X_1 \cdot X_2 \cdot X_3 < 1 \end{cases} \quad (A.15)$$

And ultimately:

$$\ln\left(\frac{\delta^{18}O_{SO_{4(A.E)}} - \delta^{18}O_{SO_4}}{\delta^{18}O_{SO_{4(A.E)}} - \delta^{18}O_{SO_{4(0)}}}\right) = -\theta_0 \cdot \frac{\delta^{34}S_{SO_4} - \delta^{34}S_{SO4(0)}}{\varepsilon^{34}S_{total}} \quad (A.14)$$

This relationship should be conserved at higher reaction complexity (e.g. the reaction presented in Fig. 1—Brunner et al., 2005, 2012 and according to a numerical solution in those works that is not presented here).

Based on these assumptions, the solution for $\delta^{18}O_{SO_4}$ with initial conditions at $t = 0$, $\delta^{18}O_{SO_{4(t=0)}} = \delta^{18}O_{SO_{4(0)}}$ and $\delta^{34}S_{SO_{4(t=0)}} = \delta^{34}S_{SO_{4(0)}}$ for $\delta^{18}O_{SO_{4(t)}}$ and $\delta^{34}S_{SO_{4(t)}}$ yields the continuous solution for $\delta^{18}O_{SO_{4(t)}}$ (After Brunner et al., 2012):

where $\delta^{18}O_{SO_{4(t)}}$ is the oxygen isotopic composition of the residual sulfate at time t, $\delta^{18}O_{SO_{4(A.E)}}$ is the oxygen isotopic composition of the residual sulfate at apparent equilibrium (see Section 1.2 above) and $\delta^{18}O_{SO_{4(0)}}$ is the oxygen isotope composition of the initial sulfate. $\delta^{34}S_{SO_{4(t)}}$ is the sulfur isotopic composition of the residual sulfate at time t, $\delta^{34}S_{SO_{4(0)}}$ is the initial sulfur isotopic composition of the residual sulfate, $\varepsilon^{34}S_{total}$ $\varepsilon^{18}O_{total}$ are the overall expressed sulfur and oxygen isotope fractionation, respectively, and θ_0 is a parameter initially formulated by Brunner et al. (2005). According to Brunner et al. (2005), this parameter (θ_0) measures the ratio between the apparent oxygen isotope exchange and sulfate reduction rate. However, since we assumed instantaneous isotopic equilibrium with the ambient water, in our case this parameter should only be a function of the ratio between the backward and forward fluxes, and is less impacted by changes in the initial isotopic composition of the sulfate, the isotopic composition of the water, the kinetic isotope fractionation factor for step 3, or the magnitude of the fractionation factor during oxygen isotopic exchange (Brunner et al. (2012)).

APPENDIX B. MODIFICATION OF THE APPARENT EQUILIBRIUM

Considering the reaction as in Fig. 3:

At steady state:

$$\frac{d}{dt}({SO_{4(ex)}}^{2-}) = -f_1 + b_1$$
$$\frac{d}{dt}({SO_{4(in)}}^{2-}) = 0$$
$$-f_1 + b_1 = -f_3 + b_3$$

The mass balance equation for $\delta^{18}O_{SO_{4(ex)}}$:

$$\frac{d}{dt}({SO_{4(ex)}}^{2-} \cdot \delta^{18}O_{SO_{4(ex)}}) = -f_1 \cdot (\delta^{18}O_{SO_{4(ex)}} - \varepsilon^{18}O_{f\_1}) + b_2 \cdot (\delta^{18}O_{SO_{4(in)}}) \quad (B.1)$$

The mass balance equation for $\delta^{18}O_{SO_{4(in)}}$:

$$\frac{d}{dt}({SO_{4(in)}}^{2-} \cdot \delta^{18}O_{SO_{4(in)}}) = f_1 \cdot (\delta^{18}O_{SO_{4(ex)}} - \varepsilon^{18}O_{f\_1}) - b_1 \cdot (\delta^{18}O_{SO_{4(in)}}) \cdots - f_3 \cdot (\delta^{18}O_{SO_{4(in)}} - \varepsilon^{18}O_{f\_3}) + b_3 \cdot (\delta^{18}O_{H2O} + \varepsilon^{18}O_{exchange}) \quad (B.2)$$

At apparent equilibrium the change with time of $\delta^{18}O_{SO_{4(ex)}}$, $\delta^{18}O_{SO_{4(in)}}$ and $SO^{-2}_{4(in)}$ are equal 0 and therefore; Eq. (A.2.1) can be written as:

$$\delta^{18}O_{SO_{4(ex)}} - \frac{f_1}{f_2}\varepsilon^{18}O_{f\_1} = \delta^{18}O_{SO_{4(in)}} \quad (B.3)$$

And Eq. (B.2) can be written as:

$$-f_1 \cdot (\delta^{18}O_{SO_{4(ex)}} - \varepsilon^{18}O_{f\_1}) + b_1 \cdot (\delta^{18}O_{SO_{4(in)}}) = -f_3 \cdot (\delta^{18}O_{SO_{4(in)}} - \varepsilon^{18}O_{f\_3}) + b_3 \cdot (\delta^{18}O_{H2O} + \varepsilon^{18}O_{exchange}) \quad (B.4)$$

Combination of Eqs. (B.3) and (B.4) and the Steady state conditions results in the modified term for apparent equilibrium:

$$\delta^{18}O_{SO_{4(ex)}} = \delta^{18}O_{H2O} + \varepsilon^{18}O_{exchange} + \frac{\varepsilon^{18}O_{f\_3}}{X_3} + \frac{\varepsilon^{18}O_{f\_1}}{X_1 \cdot X_3} \quad (B.5)$$

APPENDIX C. OPEN SYSTEM MODEL DESCRIPTION

In order to investigate to what extent the closed system model can be apply to an open system (such as natural environmental pore fluids), we generated sulfate, $\delta^{18}O_{SO_4}$ and $\delta^{34}S_{SO_4}$ synthetic profiles for two extreme cases in this study, deep sea sedimentary pore fluids and estuarine sedimentary pore fluids. The profiles were generated using the general diagenetic equation (Berner, 1980):

$$\frac{\partial \varphi C_i}{\partial t} = \varphi \frac{\partial}{\partial Z}\left(D_s \frac{\partial C_i}{\partial Z}\right) - \varphi(U + \omega)\frac{\partial C_i}{\partial z} - \Sigma R_i \quad (C.1)$$

where C_i represents each of the different sulfate isotopologues (in our case $^{32}S^{16}O_4^{2-}$, $^{34}S^{16}O_4^{2-}$, $S^{18}O^{16}O_3^{2-}$ as we considered all other species as much less abundant) consecrations in mass per unit volume of total sediment, t is time, Z is the depth in unit length, ϕ is the porosity , D_s is the diffusion coefficient in unite of length square per time, U is the velocity of flow relative to the sediment-water interface in units of length per time, ω is the rate of burial of the layer below the sediment-water interface in units of length per time and R_i is the reaction rate in units of mass

per volume per time. .For our purpose we assume no advection and uniform porosity throughout the sediment column. In addition the sulfate reduction rates were considered as constant in space and time (the SRR of each sulfate species was calculated using the overall SRR and the expected change in $\delta^{18}O_{SO_{4(t=0)}}$ and $\delta^{34}S_{SO_4}$ according to our close system model—see Section 4). Therefore Eq. (C.1) can be written as:

$$\varphi \frac{\partial C_i}{\partial t} = \varphi \cdot D_s \frac{\partial^2 C_i}{\partial X^2} - \varphi \cdot \omega \frac{\partial C_i}{\partial z} - \mathrm{SRR}_{(Ci)} \qquad \text{(C.2)}$$

We solved Eq. (C.2) using finite difference. The concentration of the sulfate species isotopologues were initiated from seawater values throughout the entire sediment. The concentrations at the top and the bottom of the sediment were fixed to the initial concentration as boundary conditions. We let the profiles reach steady state (we define steady state when the maximum different between the concentrations two time intervals at given depth is smaller than 10 orders of magnitudes than the concentration at this depth). The parameters that been used for each on of the cases in order to solved Eq. (C.2) are given in Table EA.1.

APPENDIX D. SUPPLEMENTARY DATA

Supplementary data associated with this article can be found, in the online version, at http://dx.doi.org/10.1016/j.gca.2013.05.005.

REFERENCES

Aharon P. and Fu B. (2000) Microbial sulfate reduction rates and sulfur and oxygen isotope fractionations at oil and gas seeps in deepwater Gulf of Mexico. *Geochim. Cosmochim. Acta* **64**(2), 233–246.

Aharon P. and Fu B. (2003) Sulfur and oxygen isotopes of coeval sulfate–sulfide in pore fluids of cold seep sediments with sharp redox gradients. *Chem. Geol.* **195**, 201–218.

Aller R. C. and Blair N. E. (1996) Sulfur diagenesis and burial on the Amazon Shelf: major control by physical sedimentation processes. *Geol. Mar. Lett.* **16**, 3–10.

Aller R. C., Madrid V., Chistoserdov A., Aller J. Y. and Heilbrun C. (2010) Unsteady diagenetic processes and sulfur biogeochemistry in tropical deltaic muds: implications for oceanic isotope cycles and the sedimentary record. *Geochim. Cosmochim. Acta* **74**, 4671–4692.

Balci N., Shanks W., Bernhard M. and Mandernack K. (2007) Oxygen and sulfur isotope systematics of sulfate produced by bacterial and abiotic oxidation of pyrite. *Geochim. Cosmochim. Acta* **71**, 3796–3811.

Berner R. A. (1980) *Early Diagenesis: A Theoretical Approach*. Princeton University Press.

Betts R. H. and Voss R. H. (1970) The kinetics of oxygen exchange between the sulfite ion and water. *Can. J. Chem.* **48**, 2035–2041.

Blake R. E., Surkov A. V., Böttcher M. E., Ferdelman T. G. and Jørgensen B. B. (2006) Oxygen isotope composition of dissolved sulfate in deep-sea sediments: Eastern Equatorial Pacific Ocean. In *Proceedings of the Ocean Drilling Programm, Scientific Results*, Vol. 201 (eds. B. B. Jørgensen, S. L. D'Hondt and D. J. Miller). ODP, pp. 1–24.

Booth I. R. (1985) Regulation of cytoplasmic pH in bacteria. *Microbiol. Rev.* **49**, 359–378.

Böttcher M. E. and Thamdrup B. (2001) Anaerobic sulfide oxidation and stable isotope fractionation associated with bacterial sulfur disproportionation in the presence of MnO_2. *Geochim. Cosmochim. Acta* **65**, 1573–1581.

Böttcher M. E., Brumsack H. J. and de Lange G. J. (1998) Sulfate reduction and related stable isotope (^{34}S, ^{18}O) variations in interstitial waters from the eastern Mediterranean. In *Proc. ODP, Sci. Results*, Vol. 16 (eds. A. H. F. Robertson, K.-C. Emeis, C. Richter and A. Camerlenghi). College Station, TX, Ocean Drilling Program, pp. 365–373.

Böttcher M. E., Bernasconi S. M. and Brumsack H. J. (1999) Carbon, sulfur, and oxygen isotope geochemistry of interstitial waters from the western Mediterranean. In *Proceedings of the Ocean Drilling Program, Scientific Results*, Vol. 161 (eds. R. Zahn, M. C. Comas and A. Klaus). College Station, TX, Ocean Drilling Program, pp. 413–421.

Böttcher M. E., Thamdrup B. and Vennemann T. W. (2001) Oxygen and sulfur isotope fractionation during anaerobic bacterial disproportionation of elemental sulfur. *Geochim. Cosmochim. Acta* **65**, 1601–1609.

Böttcher M. E., Thamdrup B., Gehre M. and Theune A. (2005) $^{34}S/^{32}S$ and $^{18}O/^{16}O$ Fractionation during sulfur disproportionation by *Desulfobulbus propionicus*. *Geomicrobiol. J.* **22**, 219.

Böttcher M. E., Ferdelman T. G., Jørgensen B. B., Blake R. E., Surkov A. V. and Claypool G. E. (2006) Sulfur isotope fractionation by the deep biosphere within sediments of the Eastern Equatorial Pacific and Peru Margin. In *Proceedings of the Ocean Drilling Program, Scientific Results*, Vol. 201 (eds. B. B. Jørgensen, S. L. D'Hondt and D. J. Miller). ODP, pp. 1–21.

Bradley A. S., Leavitt W. D. and Johnston D. T. (2011) Revisiting the dissimilatory sulfate reduction pathway. *Geobiology* **9**, 446–457.

Brüchert V. (2004) Physiological and ecological aspects of sulfur isotope fractionation during bacterial sulfate reduction. In *Sulfur Biogeochemistry – Past and Present*, Vol. 379 (eds. J. P. Amend, K. J. Edwards and T. W. Lyons): Geological Society of America Special Paper. Geological Society of America, Boulder CO, USA, pp. 1–16.

Brüchert V., Knoblauch C. and Jørgensen B. B. (2001) Microbial controls on the stable sulfur isotopic fractionation during bacterial sulfate reduction in Arctic sediments. *Geochim. Cosmochim. Acta* **65**, 753–766.

Brunner B. and Bernasconi S. M. (2005) A revised isotope fractionation model for dissimilatory sulfate reducing in sulfate reducing bacteria. *Geochim. Cosmochim. Acta* **69**, 4759–4771.

Brunner B., Bernasconi S. M., Kleikemper J. and Schroth M. J. (2005) A model for oxygen and sulfur isotope fractionation in sulfate during bacterial sulfate reduction processes. *Geochim. Cosmochim. Acta* **69**, 4773–4785.

Brunner B., Mielke R. E. and Coleman M. (2006) Abiotic oxygen isotope equilibrium fractionation between sulfite and water. American Geophysical Union, Fall Meeting 2006, Eos Trans AGU 87 (abstr. V11C-0601).

Brunner B., Yu J.-Y., Mielke R., MacAskill J., Madzunkov S., McGenity T. and Coleman M. (2008) Different isotope and chemical patterns of pyrite oxidation related to lag and exponential growth phases of *Acidithiobacillus ferrooxidans* reveal a microbial growth strategy. *Earth Planet. Sci. Lett.* **270**, 63–72.

Brunner B., Einsiedl F., Arnold G. L., Müller I., Templer S. and Bernasconi S. (2012) The reversibility of dissimilatory sulphate reduction and the cell-internal multistep reduction of sulphite to sulphide: insights from the oxygen isotope composition of sulphate. *Isotopes in Environmental & Health Studies* **48**, 33–54.

Canfield D. E. (2001a) Biogeochemistry of sulfur isotopes. In *Reviews in Mineralogy and Geochemistry*, Vol. 43 (eds. J. W.

Valley and D. R. Cole). Blacksburg, VA, Mineralogical Society of America, pp. 607–636.

Canfield D. E. (2001b) Isotope fractionation by natural populations of sulfate-reducing bacteria. *Geochim. Cosmochim. Acta* **65**, 1117–1124.

Canfield D. E. and Thamdrup B. (1994) The production of ^{34}S-depleted sulfide during bacterial disproportionation of elemental sulfur. *Science* **266**, 1973–1975.

Canfield D. E., Olesen C. A. and Cox R. P. (2006) Temperature and its control of isotope fractionation by a sulfate-reducing bacterium. *Geochim. Cosmochim. Acta* **70**, 548–561.

Chambers L. A., Trudinger P. A., Smith J. W. and Burns M. S. (1975) Fractionation of sulfur isotopes by continuous cultures of Desulfovibrio desulfuricans. *Canadian Journal of Microbiology* **21**, 1602–1607.

Chernyavsky B. M. and Wortmann U. G. (2007) REMAP: A reaction transport model for isotope ratio calculations in porous media. *Geochemistry, Geophysics, Geosystems* **8**, Q02009.

Chiba H. and Sakai H. (1985) Oxygen isotope exchange-rate between dissolved sulfate and water at hydrothermal temperatures. *Geochim. Cosmochim. Acta* **49**, 993–1000.

Cypionka H., Smock A. and Böttcher M. E. (1998) A combined pathway of sulfur compound disproportionation in *Desulfovibrio desulfuricans*. *FEMS Microbiol. Lett.* **166**, 181–186.

D'Hondt S., Jørgensen B. B., Miller D. J., Batzke A., Blake R., Cragg B. A., Cypionka H., Dickens G. R., Ferdelman T., Hinrichs K., Holm N. G., Mitterer R., Spivack A., Wang G., Bekins B., Engelen B., Ford K., Gettemy G., Rutherford S. D., Sass H., Skilbeck C. G., Aiello I. W., Guèrin G., House C. H., Inagaki F., Meister P., Naehr T., Niitsuma S., Parkes R. J., Schippers A., Smith D. C., Teske A., Wiegel J., Padilla C. N. and Acosta J. L. S. (2004) Distributions of microbial activities in deep subseafloor sediments. *Science* **306**, 2216–2221.

Donahue M. A., Werne J. P., Meile C. and Lyons T. W. (2008) Modeling sulfur isotope fractionation and differential diffusion during sulfate reduction in sediments of the Cariaco Basin. *Geochim. Cosmochim. Acta* **72**, 2287–2297.

Eckert T., Brunner B., Edwards E. A. and Wortmann U. G. (2011) Microbially mediated re-oxidation of sulfide during dissimilatory sulfate reduction by *Desulfobacter latus*. *Geochim. Cosmochim. Acta* **75**, 3469–3485.

Farquhar J., Johnston D. T., Wing B. A., Habicht K. S., Canfield D. E., Airieau S. and Thiemens M. H. (2003) Multiple sulphur isotopic interpretations of biosynthetic pathways: implications for biological signatures in the sulphur isotope record. *Geobiology* **1**, 27–36.

Farquhar J., Johnston D. T. and Wing B. A. (2007) Implications of conservation of mass effects on mass-dependent isotope fractionations: influence of network structure on sulfur isotope phase space of dissimilatory sulfate reduction. *Geochim. Cosmochim. Acta* **71**, 5862–5875.

Farquhar J., Canfield D. E., Masterson A., Bao H. and Johnston D. (2008) Sulfur and oxygen isotope study of sulfate reduction in experiments with natural populations from F_llestrand, Denmark. *Geochim. Cosmochim. Acta* **72**, 2805–2821.

Fritz P., Basharmal G. M., Drimmie R. J., Ibsen J. and Qureshi R. M. (1989) Oxygen isotope exchange between sulfate and water during bacterial reduction of sulfate. *Chem. Geol.* **79**, 99–105.

Froelich P., Klinkhammer G., Bender M., Luedtke N., Heath G. R., Cullen D., Dauphin P., Hammond D., Hartman B. and Maynard V. (1979) Early oxidation of organic matter in pelagic sediments of the eastern equatorial Atlantic: suboxic diagenesis. *Geochim. Cosmochim. Acta* **43**, 1075–1090.

Greene E. A., Hubert C., Nemati M., Jenneman G. E. and Voordouw G. (2003) Nitrite reductase activity of sulphate-reducing bacteria prevents their inhibition by nitrate-reducing, sulphide-oxidizing bacteria. *Environ. Microbiol.* **5**, 607–617.

Harrison A. G. and Thode H. G. (1958) Mechanism of the bacterial reduction of sulphate from isotope fractionation studies. *Trans. Faraday Soc.* **53**, 84–92.

Habicht K. S. and Canfield D. E. (1996) Sulphur isotope fractionation in modern microbial mats and the evolution of the sulphur cycle. *Nature* **382**, 342–343.

Habicht K. S., Gade M., Thamdrup B., Berg P. and Canfield D. E. (2002) Calibration of sulphate levels in the Archean Ocean. *Science* **298**, 2372–2374.

Heidel C. and Tichomirowa M. (2011) The isotopic composition of sulfate from anaerobic and low oxygen pyrite oxidation experimenzs with ferric iron – new insights into oxidation mechanisms. *Chem. Geol.* **281**, 305–316.

Holler T., Wegener G., Niemann H., Deusner C., Ferdelman T. G., Boetius A., Brunner B. and Widdel F. (2011) Carbon and sulfur back flux during anaerobic microbial oxidation of methane and coupled sulfate reduction. *Proc. Natl. Acad. Sci. U.S.A.* **108**, 1484–1490.

Horner D. A. and Connick R. E. (2003) Kinetics of oxygen exchange between the two isomers of bisulfite ion, disulfite ion ($S_2O_5^{2-}$), and water as studied by oxygen-17 Nuclear Magnetic Resonance Spectroscopy. *Inorg. Chem.* **42**, 1884–1894.

Johnston D. T., Farquhar J. and Canfield D. E. (2007) Sulfur isotope insights into microbial sulfate reduction: when microbes meet model. *Geochim. Cosmochim. Acta* **71**, 3929–3947.

Jørgensen B. B. (1979) A theoretical model of the stable sulfur isotope distribution in marine sediments. *Geochim. Cosmochim. Acta* **43**, 363–374.

Kaplan I. R. and Rittenberg S. C. (1964) Microbiological fractionation of sulphur isotopes. *J. Gen. Microbiol.* **34**, 195–212.

Kasten S. and Jørgensen B. B. (2000) Sulfate reduction in marine sediments. In *Marine Geochemistry* (eds. H. D. Schulz and M Zabel). Springer, Berlin, pp. 263–281.

Kobayashi K., Tachibana S. and Ishimoto M. (1969) Intermediary formation of trithionate in sulfite reduction by a sulfate-reducing bacterium. *J. Biochem. (Tokyo)* **65**, 155.

Kohl I. E. and Bao H. (2006) Does enzyme-catalyzed formation of sulfate complexes cause oxygen isotope exchange during dissimilatory microbial sulfate reduction? *Eos Trans. AGU* **87**, V11C-0599.

Kohl I. E. and Bao H. (2011) Triple-oxygen-isotope determination of molecular oxygen incorporation in sulfate produced during abiotic pyrite oxidation (pH = 2–11). *Geochim. Cosmochim. Acta* **75**, 1785–1798.

Kohl I. E., Asatryan R. and Bao H. (2012) No oxygen isotope exchange between water and APS–sulfate at surface temperature: evidence from quantum chemical modeling and triple-oxygen isotope experiments. *Geochim. Cosmochim. Acta* **95**, 106–118.

Knöller K., Vogt C., Richnow H. H. and Weise S. M. (2006) Sulfur and oxygen isotope fractionation during benzene, toluene, ethyl benzene, and xylene degradation by sulfate-reducing bacteria. *Environmental Science & Technology* **40**, 3879–3885.

Lloyd R. M. (1968) Oxygen isotope behavior in sulfate–water system. *J. Geophys. Res.* **73**, 6099–6110.

Mandernack K., Krouse H. R. and Skei J. M. (2003) A stable sulfur and oxygen isotopic investigation of sulfur cycling in an anoxic marine basin, Framvaren Fjord, Norway. *Chem. Geol.* **195**, 181–200.

Mangalo M., Meckenstock R. U., Stichler W. and Einsiedl F. (2007) Stable isotope fractionation during bacterial sulfate reduction is controlled by reoxidation of intermediates. *Geochim. Cosmochim. Acta* **71**, 4161–4171.

Mangalo M., Einsiedl F., Meckenstock R. U. and Stichler W. (2008) Influence of the enzyme dissimilatory sulfite reductase on stable isotope fractionation during sulfate reduction. *Geochim. Cosmochim. Acta* **71**, 4161–4171.

Mizutani Y. and Rafter T. A. (1969) Oxygen isotopic composition of sulphates – Part 4; bacterial fractionation of oxygen isotopes in the reduction of sulphates and in the oxidation of sulphur. *N. Z. J. Sci.* **12**, 60–68.

Mizutani Y. and Rafter T. A. (1973) Isotopic behavior of sulphate oxygen in the bacterial reduction of sulphate. *Geochem. J.* **6**, 183–191.

Niewöhner C., Hensen C., Kasten S., Zabel M. and Schulz H. D. (1998) Deep sulfate reduction completely mediated by anaerobic methane oxidation in sediments of the upwelling area off Namibia. *Geochim. Cosmochim. Acta* **62**, 455–464.

Reeburgh W. S. (2007) Oceanic methane biogeochemistry. *Chem. Rev.* **107**, 486–513.

Rees C. E. (1973) A steady-state model for sulphur isotope fractionation in bacterial reduction processes. *Geochim. Cosmochim. Acta* **37**, 1141–1162.

Sim M. S., Bosak T. and Ono S. (2011a) Large sulfur isotope fractionation does not require disproportionation. *Science* **333**, 74–77.

Sim M. S., Ono S., Donovan K., Templer S. P. and Bosak T. (2011b) Effect of electron donors on the fractionation of sulfur isotopes by a marine *Desulfovibrio* sp.. *Geochim. Cosmochim. Acta* **75**, 4244–4259.

Stam M. C., Mason P. R. D., Laverman A. M., Pallud C. and Cappellen P. V. (2011) $^{34}S/^{32}S$ fractionation by sulfate-reducing microbial communities in estuarine sediments. *Geochim. Cosmochim. Acta* **75**, 3903–3914.

Tapgaar I. H., Røy H. and Jørgensen B. B. (2011) Concurrent low- and high-affinity sulfate reduction kinetics in marine sediment. *Geochim. Cosmochim. Acta* **75**, 2997–3010.

Trudinger P. A. and Chambers L. A. (1973) Reversibility of bacterial sulfate redaction and its relevance to isotope fractionation. *Geochimica et Cosmochimica Acta* **37**, 1775–1778.

Turchyn A. V., Sivan O. and Schrag D. (2006) Oxygen isotopic composition of sulfate in deep sea pore fluid: evidence for rapid sulfur cycling. *Geobiology* **4**, 191–201.

Turchyn A. V., Brüchert V., Lyons T. W., Engel G. S., Balci N., Schrag D. P. and Brunner B. (2010) Kinetic oxygen isotope effects during dissimilatory sulfate reduction: a combined theoretical and experimental approach. *Geochim. Cosmochim. Acta* **74**, 2011–2024.

Vossmeyer A., Deusner C., Kato C., Inagaki F. and Ferdelman T. G. (2012) Substrate specific pressure-dependence of microbial sulfate reduction in deep-sea cold seep sediments of the Japan Trench. *Front. Microbiol.* **3**, 253.

Westrich J. T. and Berner R. B. (1984) The role of sedimentary organic matter in bacterial sulfate reduction: the *G* model tested. *Limnol. Oceanogr.* **29**, 236–249.

Wortmann U. G., Bernasconi S. M. and Böttcher M. E. (2001) Hypersulfidic deep biosphere indicates extreme sulfur isotope fractionation during single-step microbial sulfate reduction. *Geology* **29**, 647–650.

Wortmann U. G. (2006) A 300 m long depth profile of metabolic activity of sulfate reducing bacteria in the continental margin sediments of South Australia (ODP Site 1130) derived from inverse reaction-transport modeling. *Geochem. Geophys. Geosyst.* **7**, Q05012.

Wortmann U. G., Chernyavsky B., Bernasconi S. M., Brunner B., Böttcher M. E. and Swart P. K. (2007) Oxygen isotope biogeochemistry of pore water sulfate in the deep biosphere: dominance of isotope exchange reactions with ambient water during microbial sulfate reduction (ODP Site 1130). *Geochim. Cosmochim. Acta* **71**, 4221–4232.

Wortmann U. G. and Chernyavsky B. M. (2011) The significance of isotope specific diffusion coefficients for reaction-transport models of sulfate reduction in marine sediments. *Geochim. Cosmochim. Acta* **75**, 3046–3056.

Zak I., Sakai H. and Kaplan I. R. (1980) Factors controlling the $^{18}O/^{16}O$ and $^{34}S/^{32}S$ isotope ratios of ocean sulfates, evaporates and interstitial sulfates from modern deep sea sediments. In *Isotope Marine Chemistry*. Institute of Geophysics and Planetary Physics, University of California Los Angeles, California, USA, pp. 339–373 (chapter 17).

Zeebe R. E. (2010) A new value for the stable oxygen isotope fractionation between dissolved sulfate ion and water. *Geochim. Cosmochim. Acta* **74**, 818–828.

Associate editor: Josef P. Werne